



## Tracking vehicle trajectories and fuel rates in phantom traffic jams: Methodology and data



Fangyu Wu<sup>a</sup>, Raphael E. Stern<sup>b,f</sup>, Shumo Cui<sup>c</sup>, Maria Laura Delle Monache<sup>d</sup>, Rahul Bhadani<sup>e</sup>, Matt Bunting<sup>e</sup>, Miles Churchill<sup>b</sup>, Nathaniel Hamilton<sup>f</sup>, R'mani Haulcy<sup>g</sup>, Benedetto Piccoli<sup>h</sup>, Benjamin Seibold<sup>c</sup>, Jonathan Sprinkle<sup>e</sup>, Daniel B. Work<sup>f,\*</sup>

<sup>a</sup> Department of Electrical Engineering and Computer Science, University of California, Berkeley, 652 Sutardja Dai Hall, Berkeley, CA 94720, USA

<sup>b</sup> Department of Civil and Environmental Engineering, University of Illinois at Urbana-Champaign, 205 N. Mathews Ave, Urbana, IL 61801, USA

<sup>c</sup> Department of Mathematics, Temple University, 1805 North Broad Street, Philadelphia, PA 19122, USA

<sup>d</sup> Inria, University Grenoble Alpes, CNRS, GIPSA-lab, F-38000 Grenoble, France

<sup>e</sup> Electrical and Computer Engineering, University of Arizona, Tucson, AZ 85721-0104, USA

<sup>f</sup> Institute for Software Integrated Systems, Vanderbilt University, 1025 16th Avenue South, Nashville, TN 37212, USA

<sup>g</sup> Yale University, New Haven, CT 06520, USA

<sup>h</sup> Department of Mathematical Sciences, Rutgers University – Camden, 311 N. 5th St, Camden, NJ 08102, USA

### ARTICLE INFO

#### Keywords:

Traffic waves and fuel consumption

Vehicle trajectories

Computer vision

Open data

### ABSTRACT

The traffic experiment conducted by Sugiyama et al. (2007) has been a seminal work in transportation research. In the experiment, a group of vehicles are instructed to drive on a circular track starting with uniform spacing. The isolated experimental environment provides a safe, economic, and controlled environment to study free flow traffic and phantom traffic waves. This article introduces a novel method that automates the data collection process in such an environment. Specifically, the vehicle trajectories are measured using a 360-degree camera, and the fuel rates are recorded via on-board diagnostics (OBD-II) scanners. The video data from the 360-degree camera is then processed by an offline unsupervised computer vision algorithm. To validate the data collection method, the technique is then evaluated on a series of eight experiments. Analysis shows that the collected data are highly accurate, with a mean positional bias of less than 0.002 m and a small standard deviation of 0.11 m. The positional data also yields reliable velocity estimates: the derived velocities are biased by only 0.02 m/s with a small standard deviation of 0.09 m/s. The produced trajectory and fuel rate data can be readily used to study human driving behaviors, to calibrate microsimulation models, to develop fuel consumption models, and to investigate engine emissions. To facilitate future research, the source code and the data are made publicly available online.

### 1. Introduction

For many decades, the collection and interpretation of empirical traffic data has shaped our understanding of vehicular interactions and traffic flow. In this paper, we aim to contribute to this subdomain by providing a novel data collection method and a set of high-quality traffic data. We begin with a brief introduction of this subject.

\* Corresponding author.

E-mail address: [dan.work@vanderbilt.edu](mailto:dan.work@vanderbilt.edu) (D.B. Work).

### 1.1. Background

The first major data collection effort to better understand traffic flow began with the pioneering experiments conducted by [Greenshields \(1934\)](#), which provided an empirical model that explained the relationship between density and velocity of traffic and, consequently, the construction of the fundamental diagram. Since then, the collection of traffic data has been a critical part of transportation research. In this work, we aim to contribute to such research efforts by providing a novel data collection method and a high-fidelity traffic dataset collected using the developed method.

Other early data collection efforts include those by researchers at *General Motors* (GM) who conducted many experiments to study vehicle-following characteristics in the 1950s and the 1960s ([Rothery et al., 1964](#); [Gerlough and Huber, 1975](#); [Gazis et al., 1959](#); [Herman and Potts, 1959](#); [Chandler et al., 1958](#)). For example, in 1958, GM conducted a series of experiments to test a car-following model, where a 1957 Oldsmobile was instructed to follow a lead car on a track at the General Motors Technical Center. This, and other early experiments, focused on the characteristics of single-lane car following behavior. To measure spacing, the researchers developed the GM *car follower*, which was a physical wire kept under tension that connected the follower and the leader and recorded the distance between the two vehicles via an oscilloscope. The readings were then manually processed to produce speed and acceleration measurements. Additional experiments conducted in this period are reviewed by [Rothery \(2001\)](#).

In the late 1960s and 1970s automated systems were deployed to collect aggregated data for the purpose of traffic monitoring and control in the Lincoln Tunnel ([Gazis and Foote, 1969](#)) and traffic estimations on the Long Island Expressway in New York ([Nahi and Trivedi, 1973](#)). Today, the shape of fundamental diagrams and more broadly the aggregated or macroscopic dynamics of traffic are greatly aided by the abundance of traffic data measured from fixed sensors such as inductive loop detectors, radars, and video cameras. One prevalent traffic data source in California is the *Performance Measurement System* (PeMS) database ([PEMS, 2018](#)). This database collects data from nearly 40,000 inductive loop detectors and toll tag readers in the state of California. Besides, the Grenoble Traffic lab instrumented a road in Grenoble, France with magnetic sensors embedded in the roadway to collect vehicle counts ([De Wit et al., 2015](#)). The Minnesota Traffic Observatory uses radar and video detectors on the I-35W/I-94 freeway to collect vehicle counts ([Observatory, 2017](#)). The Berkeley Highway Lab collected traffic counts using loop detectors on I-80 in Emeryville, CA ([May et al., 2003](#)). Such systems typically provide vehicle counts or flows, time averaged velocities, and time averaged occupancies that enable the estimation of the traffic density.

One important limitation of aggregate traffic datasets is that they were initially introduced to collect aggregated data relevant for calibrating and validating macroscopic descriptions of the traffic flow ([Dervisoglu et al., 2009](#); [Dervisoglu et al., 2014](#); [Hueper et al., 2009](#); [Zeroual et al., 2015](#); [Ranjitkar et al., 2005](#)). Microscopic descriptions of traffic ([Bando et al., 1995](#); [Helbing and Tilch, 1998](#); [Hwasoo and Skabardonis, 2009](#); [Orosz et al., 2009](#); [Tordeux and Seyfried, 2014](#); [Hoogendoorn et al., 2006](#)) can be challenging to validate in detail without data at the level of the individual vehicle.

In parallel with the aggregated data collection efforts, early efforts aimed at measuring individual vehicle trajectories on real freeways include the work of [Treiterer et al. \(1975\)](#) in the 1970s. The experiments involved flying a helicopter over freeways in Ohio to photograph the traffic, which was later used to reconstruct the vehicle trajectories. The experiments by Treiterer served as the first in a series of larger efforts to collect freeway vehicle trajectories. [Coifman \(1997\)](#) collected trajectories using a video camera on a 120 m segment of I-680 in California and observed the development of shockwaves. Other US Federal Highway Administration efforts used video footage from an aircraft to collect vehicle trajectories at six types of freeway bottleneck sections ([Smith, 1985](#)). Researchers at Delft University used cameras mounted on a helicopter to collect vehicle trajectory data on a 520 m freeway segment ([Schreuder et al., 2003](#)) in Utrecht. The aforementioned Berkeley Highway Lab ([May et al., 2003](#)) and the Minnesota Traffic Observatory ([Observatory, 2017](#)) also include efforts to extract vehicle trajectories.

Amongst the most widely used trajectory datasets are the NGSIM datasets, which were collected “in support of traffic simulation with a primary focus on microscopic modeling” ([Federal Highway Administration, 2017](#)). The datasets contain trajectories recorded at different times on three different road segments. The first of these datasets was collected using video cameras on a 900 m segment of freeway I-80 in California over 30 min in December of 2003. Additionally, in April of 2005, three 15 min data collections were performed on a 500 m segment of the same highway. Also in 2005, a 640 m segment of US-101 in Los Angeles was instrumented, and three consecutive 15 min datasets were recorded. Several recent works have used the NGSIM data to calibrate traffic models ([Treiber et al., 2008](#); [Piccoli et al., 2015](#); [Fang et al., 2014](#); [Duong et al., 2010](#); [Lu et al., 2009](#); [Kesting and Treiber, 2008a](#)). However, as pointed out in some recent works, there are limitations to this dataset since the acceleration and velocity measurements are prone to large errors ([Thiemann et al., 2008](#); [Montanino and Punzo, 2015](#); [Punzo et al., 2011](#)), which is further magnified to a great extent by the finite difference calculation on the successive vehicle positions. Proper data collection and processing techniques are required to address these issues ([Montanino and Punzo, 2015](#)). Other experimental efforts have been able to collect vehicle trajectories from individual vehicles in urban traffic ([Kesting and Treiber, 2008b](#); [Vasconcelos et al., 2014](#)) and instrumented platoons of vehicles ([Punzo et al., 2005](#)).

At the individual vehicle level, driver behavior has been analyzed using data collected through the *naturalistic driving study* (NDS) ([VTU, 2018](#)) by the second *Strategic Highway Research Program* (SHRP2). The SHRP2 data contain video footage and vehicle performance data from instrumented vehicles, and includes both a driver-facing and a forward-facing camera. The dataset contains over 42,300 h and 2,000,000 miles of driving. The dataset includes 82 collisions and 761 near misses, which have been used to analyze driving risks ([Foss and Goodwin, 2014](#); [Fitch et al., 2013](#); [Montgomery et al., 2014](#)). A related naturalistic driving dataset has also been created by the University of Michigan with data for nearly one million vehicle miles traveled ([UMTRI, 2018](#)). While these datasets provide extensive information about the instrumented vehicles, they do not include the same level of information regarding

all surrounding vehicles in the traffic stream. In addition, they can only be accessed by a limited number of qualified researchers due to privacy concerns.

Moreover, in 2010, with the popularity of smartphones, the *Mobile Century* project at the University of California, Berkeley collected smartphone-based GPS position data from probe vehicles on I-880 near Oakland, California (Herrera et al., 2010), but only for a subset of the total vehicles in the flow.

In microscopic modelling research where a 100% penetration rate is required, the datasets collected by Sugiyama et al. (2008) and Tadaki et al. (2013) are frequently used. In order to experimentally demonstrate the development of traffic instabilities such as phantom traffic waves even without lane changes or bottlenecks, Sugiyama, et al. designed and executed a set of experiments in 2007 (Sugiyama et al., 2008), and later in 2013 (Tadaki et al., 2013). These experiments involved between 10 and 40 vehicles on a circular track. All vehicles began with a uniform velocity and spacing, but the traffic quickly develops instabilities, i.e., phantom traffic waves. These datasets are fundamentally different from the previously mentioned traffic datasets since they include data from closed-road traffic experiments as opposed to data collected on open roadways.

This dataset, and other similar datasets (Tadaki et al., 2013; Shamoto et al., 2011; Jiang et al., 2014, 2015, 2017) are used for calibrating microscopic traffic flow models (Tordeux and Seyfried, 2014; Jiang et al., 2014; McGregor, 2013; Tian et al., 2016). For example, Jiang et al. (2014, 2015, 2017) collected vehicle trajectories from a platoon of 25 vehicles using GPS sensors and used the data to calibrate the parameters of the *Intelligent Driver Model* (IDM) (Jiang et al., 2014). Huang et al. (2018) collected vehicle-level data from an 11-car platoon. However, due to the low resolution of the GPS receiver, the vehicle position accuracy in all of these studies is limited to 1 m.

Although the experiments conducted by Sugiyama et al. (2008) and Tadaki et al. (2013) provide valuable vehicle trajectories, they do not contain any information on engine performance such as fuel rate. Fuel rate data are important when studying the effects of speed oscillations on environmental factors such as emissions. Furthermore, additional open trajectory datasets under oscillatory traffic may prove useful for calibrating traffic models and designing *autonomous vehicle* (AV) controllers (Davis, 2004; Talebpour and Mahmassani, 2016; Guériaud et al., 2016; Wang et al., 2016; Levine and Athans, 1966; Swaroop and Hedrick, 1996; Shladover, 1995; Fenton and Mayhan, 1991; Darbha and Rajagopal, 1999; Besselink and Johansson, 2017; Ioannou et al., 1993; Buehler et al., 2009; Rajamani et al., 1998; Bose and Ioannou, 2003) for driving in the presence of phantom traffic waves, or controlling the vehicle to eliminate them. To address this issue, we propose a novel data collection method and provide a high-quality dataset produced with such method. There two contributions are explained blow.

## 1.2. Contributions

We propose a novel data processing technique that achieves significantly higher spatial accuracy and temporal resolution as compared to the data collected in the seminal experiment of Sugiyama et al. (2008). Additionally, we provide a new trajectory dataset produced by this data processing method and provide the corresponding time-synchronized fuel rate data. We delineate the two contributions as follows.

The first contribution is the development of an unsupervised offline data processing technique to track the positions of multiple vehicles on a circular track. Compared to the previous data collection technique, our method is significantly more accurate and efficient. In the pioneering experiments in the work by Sugiyama et al. (2008), the position of each vehicle is accurate to within  $\pm 0.5$  m at 3 Hz, yielding a velocity error of  $\pm 3$  m/s (roughly 30% of the target vehicle velocity of 8.33 m/s) (Nakayama et al., 2009). In a follow up experiment (Tadaki et al., 2013), a laser scanner is used to locate the vehicles at a 0.16 m spatial resolution and 5 Hz temporal resolution, significantly improving the accuracy compared to the earlier test. In our work, we provide a much more accurate method to extract trajectories relying only on a 360-degree panoramic camera. While the basic building blocks of the presented method consists of standard image processing methods, the algorithmic design of the system is new. The resulting trajectories are shown to have a bias of less than 0.002 m with a standard deviation of 0.11 m; the velocity has a mean error of 0.02 m/s with a standard deviation of 0.09 m/s.

The second contribution of the work is the collection of eight experimental datasets that contain accurate and high-resolution vehicle trajectories and instantaneous fuel rates. It is important to note that accurate datasets for complex real-highway situations already exist (such as NGSIM), but certain research tasks (e.g., developing car-following models) can benefit from datasets that remove much of the noise associated with highway traffic and contain the occurrence of traffic waves caused by car-following dynamics. This study provides such a dataset. Moreover, the added fuel consumption data opens up the opportunity to study the precise relationship between traffic dynamics and fuel economy. The high accuracy and resolution of the trajectory data also provide valuable resources to study characteristic human driving behaviors at a temporal resolution of less than a tenth of a second.

The content of this article can be used for a variety of transportation research initiatives, including traffic stability analysis, microscopic model calibration, and fuel consumption modeling. It has already served as the basis for two derivative research projects: the method deployed in this paper has been applied to study the ability of a single autonomous vehicle to regulate oscillatory traffic flow (Stern et al., 2018b) as well as to investigate the impacts of phantom traffic waves in fuel efficiency and engine performance (Stern et al., 2018a).

However, it is important to acknowledge that the experimental setup, the proposed data processing technique, and the published dataset come with limitations. The single-lane closed-loop circular track is not a realistic representation of all real-world traffic phenomenon. For example, it does not include lane changing events, intersection conflicts, or low density flows. Additionally, the data processing method is not designed for deployment in real-time and complex urban environments, but rather for data collection in an experiment.

### 1.3. Organization

The remainder of the article is organized as follows. Section 2 explains the experimental setup and the experimental protocol. Section 3 describes the data collection method used to extract trajectories from a 360-degree video footage. Collected vehicle trajectory measurements are validated in Section 4, and the experimental data are presented in Section 5. This new dataset provides new opportunities in transportation research, as concluded in Section 6.

## 2. Experiments

A total of eight experiments were conducted in Tucson, Arizona in July 2016. The goals of these experiments were twofold: (i) to develop and test a method to extract high quality trajectory and fuel consumption data of vehicles in phantom traffic jams; and (ii) to investigate the extent to which a single vehicle (equivalent to a low penetration rate of vehicles on a freeway), driving differently from the remaining traffic, is able to change the traffic state. The main results of goal (i) are presented in the present work. Regarding goal (ii), in this work we provide preliminary evidence that a single vehicle is able to influence the flow, and note that the main experimental findings to support this objective are available in the companion article (Stern et al., 2018b). In the work by Stern et al. (2018b), additional experiments are conducted following the same setup described in the present article, but with the modification that a carefully controlled single autonomous vehicle is used to dissipate the phantom traffic jam when it appears. Each experiment is labeled with a letter from A to H, in the order they occurred. In each experiment drivers were given specific instructions on how to drive. The experimental setup is briefly outlined in Section 2.1 and the experimental protocol is summarized in Section 2.2.

### 2.1. Experimental setup

To test the performance of the proposed data processing method on a circular track, we re-created the results observed in the Sugiyama et al. (2008) experiment with an additional step of instrumenting each individual vehicle with a OBD-II scanner. Some experimental changes were made (track size, direction of driving) to account for larger and right-hand drive vehicles in the US compared to Japan. The track was available for a total of four hours for experimentation. Taking driver rest breaks and a driver briefing into account this allowed for three hours of testing. The time to re-set the track after each experiment was approximately 15 min, and each experiment lasted between five and 10 min.

The experiments are divided into two sets (see Table 1). In Experiments A-E, we used instruction I for which each driver is instructed to “safely follow the vehicle in front as if in rush hour traffic,” and varied the density by changing the number of vehicles on the road. We visually observe that some vehicles drive very conservatively (e.g., by leaving excessive gaps) which damped any waves that might arise. Consequently, we changed the driving instructions of all drivers to instruction II in Experiments F, G, and H, for which drivers were instructed to “drive by the same instructions as before, but in addition place an emphasis on closing the gap the vehicle in front, whenever safety permits.” The complete verbal instructions given to the drivers on-site are provided in the Appendix. Additionally, for Experiments G and H we instructed one driver (co-author M. Bunting, a member of experimental staff) to change his driving behavior during the experiment to observe the effect that a single vehicle has on the overall traffic flow.

The experiments were conducted on a circular track 260 m in circumference. The track length was selected to approximate the total unoccupied road space of the experiments conducted by Sugiyama et al. (2008). The main reason behind this experimental design was to induce phantom traffic waves. The induced phantom traffic waves are more interesting than freeflow or congested traffic, since the dynamics of phantom traffic waves are not as well understood as the dynamics of free flow and congestion. A phantom traffic wave will form when the average density is around 7 m/veh, as was shown by Sugiyama et al. (2008). If the unoccupied space is too large, there may never be a phantom traffic wave. On the other hand, if the unoccupied space is too little, the traffic will be stuck in congestion.

The track was constructed on a large paved parking lot at the Tucson Dragway in Tucson, Arizona, and selected for its smooth, even surface, and abundance of open space. The experimental track with vehicles is shown in Fig. 1a. The inside edge of the track was marked with short orange cones. Additional cones were used to mark the pre-measured location of the front tire of each car to ensure

**Table 1**

Summary of experimental setup. Instruction I is to “safely follow the vehicle in front as if in rush hour traffic”, while instructions II is to “place an emphasis on closing the gap between the front bumper and rear bumper of the vehicle in front.”. Spacing equals the length of the track divided by the number of vehicles.

Exp. no.	No. of vehicles	Instruction	Spacing (m/veh)	Duration (s)
A	20	I	13.00	416
B	20	I	13.00	442
C	22	I	11.82	388
D	21	I	12.38	480
E	19	I	13.68	333
F	19	II	13.68	175
G	21	II	12.38	587
H	22	II	11.82	545



(a) Vehicles driving with an initial uniform spacing.



(b) Vehicles driving with a non-uniform spacing, showing a traffic jam.

**Fig. 1.** An overview of the experimental setup for Experiment H.

uniform spacing at the start of the experiment.

The vehicles used for this experiment were procured from the University of Arizona's motor vehicle pool. The year, make, model, length, and nominal EPA-reported fuel rate of each vehicle used in the experiment is presented in [Table A.1](#). The vehicles used in each experiment is given in [Table A.2](#).

## 2.2. Experimental protocol

Each experiment consisted of the following phases: (i) setup; (ii) evacuation; (iii) initialize; (iv) drive; (v) stop; (vi) conclusion. During each phase, the following items were performed.

- (i) Setup: Vehicles are distributed equally according to the spacing of their front-left tire. Drivers are individually instructed to turn on their in-vehicle OBD-II scanners. Additional driver instructions (if any) are delivered to individual drivers through the window. The panoramic camera is switched on.
- (ii) Evacuation: All research team personnel evacuate the track.
- (iii) Initialize: An air horn sounds to instruct all drivers to switch gears from “park” to “drive”, without moving.
- (iv) Drive: An air horn sounds, to instruct all drivers to begin driving.
- (v) Stop: An air horn sounds, instructing drivers to come to a safe stop and switch gears into park.
- (vi) Conclusion: Experiment personnel enter the track after all vehicles have stopped. Drivers are individually instructed to turn off their in-vehicle OBD-II scanners. The central camera is switched off.

## 2.3. Experimental instruments

Each vehicle in the experiment was instrumented with an OBD-II scanner to collect vehicle data during the experiments. All vehicles sold in the United States after 1996 are required to provide vehicle performance data from the *engine control unit* (ECU) via an OBD-II port. The OBD-II data were logged using a ScanTool OBDLink LX scanner. The data provided through the OBD-II port included vehicle dynamics data such as engine speed, vehicle speed, and fuel rate as well as diagnostics data such as sensor voltage of a variety of vehicle sensors, which can be used to identify vehicle malfunction. While the OBD-II data format is standardized, due to different vehicle configurations and vehicle ages, not all vehicles reported the same data through OBD-II.

A VSN Mobil V360 panoramic video camera was used to record the motion of the vehicles, and was located at the center of the track. It has 360° horizontal field of view and 60° vertical field of view, recording at a resolution of 3840 × 640 pixels at a sampling rate of 30 Hz. The high spatial and temporal resolution of the panoramic camera enabled precise tracking of the dynamics of the vehicles in the scene. The proposed vehicle tracking algorithm is described next.

## 3. Methodology

Tracking moving objects in a sequence of images (frames) is a well established field in computer vision ([Forsyth and Ponce, 2015](#); [Blackman and Popoli, 1999](#); [Bar-Shalom et al., 2007](#)). The term tracking refers to the process of inferring the motion of one or multiple objects in a sequence of images ([Forsyth and Ponce, 2015](#)). Historically there have been two major categories of tracking techniques: *nonparametric* and *parametric* tracking ([Forsyth and Ponce, 2015](#)). A third class of methods based on deep neural networks has recently risen to popularity.

*Nonparametric tracking* methods require few assumptions on the underlying dynamics of the object to be tracked. One popular nonparametric method, known as *tracking by detection*, generates the trajectory of an object in a two-step approach. First the object

position is identified in each frame, and then the positions are linked using a proximity criteria to produce the full trajectory. Another category of nonparametric methods are referred to as *tracking by matching*. These methods reconstruct the trajectory of an object by matching a pixel representation of that object in one frame to the next, iterating over the full time span of the video. The tracking method used in this article is a variant of tracking by matching.

The second major category of tracking algorithms is *parametric tracking*, which exploits the underlying dynamical model to track the motion of objects. When the dynamical model of the object to be tracked is linear, *Kalman filters* are often applied. Otherwise, nonlinear filters such as *particle filters* are chosen for the purpose of object tracking (Forsyth and Ponce, 2015).

A third group of methods have recently emerged with the rising popularity of neural networks in artificial intelligence research. As an early example in 2013, *stacked denoising autoencoders* have been used for visual tracking (Wang et al., 2013). More recently, *convolutional neural networks* have been re-purposed for target tracking (Nam and Han, 2016). Moreover, an end-to-end tracking method based on *recurrent neural networks* has also been developed (Milan et al., 2016; Redmon et al., 2016; Liu et al., 2016).

The aforementioned tracking methods have been widely applied in the field of transportation research. Within the category of *nonparametric tracking*, examples of *tracking by detection* can be found in the works by Wu et al. (2017) and Pena-Gonzalez and Nuno-Maganda (2014). *Tracking by matching* methods are applied by Ponsa and Lpez (2007) and Lipton et al. (1998). Within the category of *parametric tracking*, applications of Kalman filtering in visual tracking can be seen in (Coifman, 1997; Aydos et al., 2009). The use of particle filtering in transportation tracking applications can be found in (Teo et al., 2014; Liu et al., 2007). Furthermore, the application of neural networks for vehicle tracking is studied by Shruthi (2011) and Zhou et al. (2016). In addition, comprehensive surveys of computer vision algorithms in transportation research can be found by Kastrinaki et al. (2003) and Buch et al. (2011).

The main challenge for tracking vehicles in the experimental setting described in Section 2 is that the vehicles may completely stop in the presence of phantom traffic waves. Because many nonparametric methods (Wu et al., 2017; Badenas and Pla, 1998) use the motion of the object to be tracked to identify the object from the background, these methods fail when the object no longer moves. Parametric methods circumvent this problem by using additional information obtained from the dynamical model (e.g., as in the Kalman filtering methods) to localize the object even when it has stopped moving. The accuracy of this approach hinges on the quality of the model specified for the object being tracked.

The tracking by matching approach, with suitable modification to handle stationary vehicles, is chosen in this work for its simplicity and effectiveness. It does not require knowledge about the underlying model of the object dynamics (in contrast to the parametric methods), nor a large training dataset (needed in supervised methods such as many neural networks applications). Although some steps in the algorithm such as background subtraction and estimation are computationally intensive, as a whole they deliver highly accurate positional estimates.

We briefly describe the general process to extract the vehicle trajectories from the camera data, which can be split into four major steps: (i) background estimation and subtraction, (ii) object identification, (iii) object tracking, and (iv) noise reduction. Given a panoramic video containing vehicles to be tracked and a nearly static background, each pixel in each frame is labeled as either *moving* or *stationary*. Moving pixels often correspond to vehicles and are unlikely to belong to the background scenery, while stationary pixels may belong to the background or to a stationary vehicle. Over a time interval containing multiple frames, an estimate of the complete background scene for the time interval can be constructed by taking a simple median (over time) of the color value of each stationary pixel. A high quality estimate of the background is obtained from the median provided that fewer than half of the frames contain stationary vehicles, which is always true in our experiments.

Vehicle trajectories are reconstructed from the video by identifying the location of each vehicle throughout the video. First a template of each vehicle is constructed. The background scene is compared to a candidate frame in the video to identify pixels that do not “match” the value in the background scene. These non-matching pixels are identified as belonging to the foreground (i.e., to a vehicle), independent of whether the vehicle is moving or stationary. These foreground pixels are then grouped into vehicles using a density-based clustering algorithm, which is further refined to define a high quality template (i.e., a picture) of the vehicle. After the template is defined, it is used to re-identify the vehicle in subsequent frames, allowing a trajectory for that vehicle to be constructed. Since the track radius is known a priori, the position of each vehicle in pixel space can be converted to a location on the track via straightforward geometry. The trajectories are further refined using a spline smoothing algorithm with outlier detection, to reduce the effects of small tracking errors and the quantization error induced by the resolution of the camera. These steps are explained in detail below.

### 3.1. Background subtraction

In this step, an estimate of the background is obtained over a sequence of frames of the video. The process of estimating the background is complicated by the facts that (i) the vehicles occlude the background scene, (ii) occasionally vehicles stop (i.e., in a phantom traffic wave), making them difficult to differentiate from the stationary background using motion-based methods, and (iii) occasionally the background changes or moves (e.g., due to changes in light intensity or the motion of clouds). Consequently, we adopt a strategy that first detects sufficiently stationary pixels in each frame (described in detail below), and we estimate the background as the median pixel value over the set of images. For an individual pixel location, the median of the non-moving pixels provides a reasonable estimate of the background pixel value as long as the majority of frames in which the pixel is stationary do not correspond to a vehicle. This condition is met in our experiments by choosing a time horizon to estimate the background which is sufficiently large relative to the duration over which vehicles are stopped in the phantom traffic wave.

Precisely, the background identification proceeds as follows. Consider a video composed of a sequence of images indexed by  $t \in \mathbb{Z}_+$ , where each image is composed of a matrix of pixels. Denote  $V(x, y, t)$  as the value of the pixel in frame  $t$  located at



**Fig. 2.** Step-by-step visualization of background subtraction methods. Layer 1 shows a section of the estimated background within the first 15-s time interval in Experiment A. Layer 2 is the first frame of that time interval. Layer 3 is the square distance between layer 1 and layer 2. Layer 4 is the remaining foreground after removing pixels at locations that have square distance under 14. Layer 5A is the refined foreground after applying morphological transformation on layer 4. Layer 5B is the refined foreground after removing noise pixels outside the alpha complex of every vehicle from layer 4.

$(x, y) \in \{1, \dots, x_{\max}\} \times \{1, \dots, y_{\max}\} = \mathcal{X} \times \mathcal{Y}$  in the scene. The parameters  $x_{\max}$  and  $y_{\max}$  denote the horizontal and vertical resolution of the camera, respectively. For RGB video,  $V(x, y, t)$  is a vector of dimension three, with each color channel (red, green, and blue) taking values in  $\{0, \dots, 255\}$ . For each pixel  $(x, y)$ , we determine whether the pixel corresponds to a moving object between frame  $t$  and  $t + 1$  using a standard implementation of *dense optical flow* (Farneback, 2003), which is a computer vision algorithm designed to detect the apparent motion of pixels across two frames. We apply dense optical flow to all consecutive image pairs between  $t$  and  $t + \Delta t$ . The output of the algorithm is an index set for each pixel  $\mathcal{S}(x, y) \subseteq \{t, \dots, t + \Delta t\}$ , which contains the frames in which pixel  $(x, y)$  is identified to be stationary. Finally, the RGB background corresponding to pixel  $(x, y)$  is denoted  $B(x, y)$  and computed as

$$B(x, y) = \text{median}\{V(x, y, \tau) \mid \tau \in \mathcal{S}(x, y)\}, \quad (1)$$

where the median is applied channel-wise.

For practical implementations such as the experiments presented in this work, the estimated background image needs to be slowly updated over time to account for slowly varying changes such as light intensity. In our present implementation, the background is recomputed every 15 s. Fig. 2 layer 1 shows the estimated static background within first 15 s of the Experiment A, as compared to Fig. 2 layer 2 which shows the first frame in the corresponding 15-s time interval, including the vehicles. It is clear from the images that foreground vehicles are completely removed from the estimated background.

After the background is defined, foreground pixels corresponding to vehicles can be identified, independent of whether the vehicle is moving or not, as those with a sufficiently different value from the background. Precisely, for each frame  $t$ , we compute the foreground pixel set as

$$\mathcal{F}(t) = \{(x, y) \in \mathcal{X} \times \mathcal{Y} \mid \|V(x, y, t) - B(x, y)\|_2 \geq \gamma\}, \quad (2)$$

where  $\gamma$  is a difference threshold below which the pixel value of the video is assumed to match the background. An example of a set of foreground pixels under the threshold parameter  $\gamma = 48$  is shown in Fig. 2 layer 4, which shows the vehicles are clearly identified as part of the foreground, along with some additional non-vehicle pixels (noise). In our testing, pixels corresponding to vehicles are identified for a range of  $\gamma$  values (e.g.,  $48 \pm 12$  pixels), and the threshold choice is not too sensitive.

The foreground set  $\mathcal{F}$  contains all pixels estimated as belonging to vehicles, which needs further refinement to eliminate the noise. For example, isolated foreground pixels are unlikely to correspond to vehicles, which typically occupy hundreds of pixels in our implementation. Two standard *morphological transformations* (i.e., erosion and dilation, see Serra (1982) for more detail) are applied, which act as filters to reduce the noise in the foreground pixel set. The refined foreground after applying these denoising steps is shown in Fig. 2 layer 5A, where the noisy pixels are substantially reduced in number.

### 3.2. Object identification

After the background has been subtracted (i.e., pixel-wise and channel-wise subtraction) from every frame, we proceed next to construct a template of each vehicle which can be tracked from one background subtracted frame to the next. A high quality template

of each vehicle is constructed on a single frame by first clustering the foreground pixels into vehicles, and then enhancing each vehicle cluster, e.g., by filling in holes. We note that keeping the vehicle template static works the best (compared to allowing the template to be adjusted as time progresses) in our experience, because it prevents the templates from being polluted by random noise. The quality of tracking can degrade substantially if the quality of input template is not maintained.

The construction of the vehicle template via clustering relies on the fact that (in the present experimental setup) the foreground pixels from the same vehicle have smaller Euclidean distance to the pixels corresponding to the same vehicle, compared to pixels from different vehicles. Consequently, a density-based clustering algorithm can effectively group those foreground pixels into clusters. An off-the-shelf unsupervised clustering algorithm known as *density-based spatial clustering of applications with noise* (DBSCAN) (Ester et al., 1996) is applied, with a small transformation to the input video data to account for the periodicity of the image recorded by the panoramic camera (i.e., the fact that pixels near  $x_0$  and  $x = x_{\max}$  can correspond to the same vehicle).

The periodicity is addressed by transforming the image into an annulus where the beginning and the end of the original image frame are connected, so that DBSCAN can be directly applied. The clustering in DBSCAN is controlled through two parameters corresponding to (i) the maximum nearest-neighbor distance of points within the same cluster  $d_{\max}$ , (ii) the minimum cluster size  $n_{\min}$ . In the present work, we set  $d_{\max}$  corresponding to 2.5 pixels and  $n_{\min} = 15$  points. These parameters are observed to generalize well across the various experiments. Finally, the pixel clusters in polar coordinates are mapped back to the Cartesian coordinates for further analysis.

Each cluster identified in DBSCAN is converted into a vehicle template by construction of the *alpha complex* of the cluster. The cluster alpha complex results in a possibly non-convex shape to define the vehicle, and can be computed via *Delaunay triangulation* of the point set (Edelsbrunner and Seidel, 1986). Any missing pixels in the interior of the alpha complex are defined as belonging to the vehicle template, and consequently missing pixels in the template are “filled in.” An example of a cluster from DBSCAN, its convex hull, and the alpha complex are shown in Fig. 3. The templates of all vehicles in Experiment A is shown in Fig. 4.

### 3.3. Object tracking

Object tracking in this application is the procedure to determine the locations of the vehicles over time. This objective can be achieved by means of frame-by-frame matching of the vehicle template to the foreground image. More precisely, the vehicle template is matched to a transformed image in which the background image has been subtracted and the resulting foreground noise is reduced using morphological operations. In the object tracking step, the RGB images are converted to a scalar greyscale quantity, so that standard implementation libraries (i.e., OpenCV (OpenCV.org, 2016)) can be used directly. The implementation details of the technique are as follows.

Let  $\mathcal{T} \subseteq \mathcal{X} \times \mathcal{Y}$  be the union of the pixels defining the vehicle and the black pixels within the vehicle’s smallest bounding box. Suppose  $T(x, y)$  is a zero-average template of the vehicle constructed in the initial frame  $t_0$ , i.e.,

$$T(x, y) = V(\tilde{x}, \tilde{y}, t_0)|_{(\tilde{x}, \tilde{y}) \in \mathcal{T}} - \frac{1}{|\mathcal{T}|} \sum_{(\tilde{x}, \tilde{y}) \in \mathcal{T}} V(\tilde{x}, \tilde{y}, t_0) \quad (3)$$

In practice, the template is constructed on frame  $t_0 = 0$  unless otherwise specified.

Let  $I(x, y, t)$  be a zero-averaged image over an area  $\mathcal{I}(t) = \{(x + \Delta x, y + \Delta y) | (x, y) \in \mathcal{T}, |\Delta x| \leq 10 \text{ px}, |\Delta y| \leq 2 \text{ px}\}$  ( $1 \text{ px} \approx 0.0667 \text{ m}$ ) at time  $t$ :

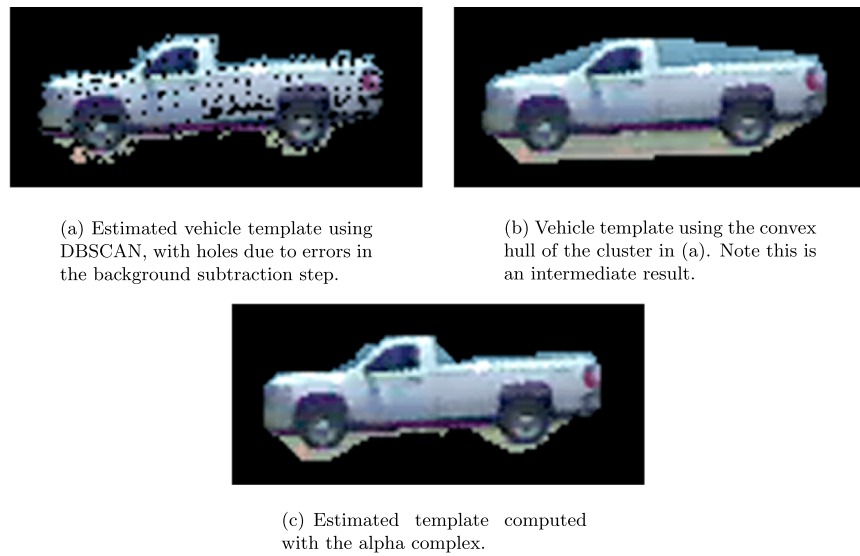


**Fig. 3.** Template construction of a pickup truck in Experiment A.

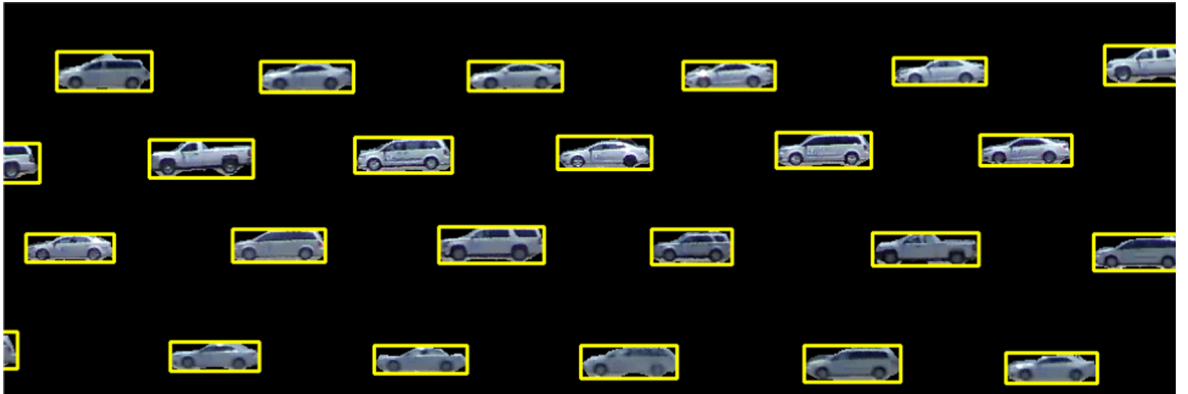


**Fig. 4.** Templates of all vehicles in Experiment A. The template of each vehicle is enclosed by a yellow bounding box, and shows the front and rear bumper locations are also accurately determined (relevant for measuring vehicle gaps). (For interpretation of the references to colour in this figure legend, the reader is referred to the web version of this article.)

$$I(x, y, t) = V(\tilde{x}, \tilde{y}, t)|_{(\tilde{x}, \tilde{y}) \in \mathcal{S}(t)} - \frac{1}{|\mathcal{S}(t)|} \sum_{(\tilde{x}, \tilde{y}) \in \mathcal{S}(t)} V(\tilde{x}, \tilde{y}, t) \quad (4)$$

We estimate the current location of the vehicle by its shift  $\Delta x$  and  $\Delta y$  using a zero-centered cross correlation function:

$$(\Delta x^*, \Delta y^*) = \operatorname{argmax}_{\Delta x, \Delta y} \sum_{(x, y) \in \mathcal{S}} I(x + \Delta x, y + \Delta y, t) \cdot T(x, y), \quad (5)$$

which is more robust than Euclidean distance measures for noisy scenes (Nakhmani and Tannenbaum, 2013).

To avoid mismatching an adjacent vehicle, we search the template only in a small neighborhood of the vehicle location identified in the previous frame, as illustrated in Fig. 5. Specifically, we restrict  $|\Delta x| \leq 10px$  and  $|\Delta y| \leq 2px$ , based on physical bounds on the vehicle velocities under small tracking errors.

Finally, the vehicle trajectories are mapped from video units into physical units. This involves converting time from frames into seconds and converting distance data from pixels into meters. Time conversion can be simply done using the fixed frame rate of 30 fps. To convert the distance measures, one can exploit the fact that the track is circular with a 260-meter circumference (at the center line of the vehicles). Hence, dividing 260 m by 3840 pixels (the width of a frame), one obtains the conversion factor of  $\frac{260}{3840} \approx 0.0667$  m/px.

### 3.4. Noise reduction

To improve the quality of the data generated from the tracking algorithm, a *basis spline* (B-spline) noise reduction method is applied. We first describe the major types of noise observed in the dataset, and then the smoothing technique used to reduce the noise.

There are two primary sources of noise in the trajectory data produced from the image processing algorithm: (i) quantization errors and (ii) burst noise. *Quantization errors* arise from the limited resolution of the panoramic camera. As a result, the distance measure is quantized to pixels, and time only advances in discrete steps of  $\frac{1}{\text{framerate}} = \frac{1}{30}$  second. If left unsmoothed, this limited spatial and temporal resolution would restrict velocity estimates to integer multiples of 30 px/s, or 2.03 m/s, and acceleration estimates to integer multiples of 900 px/s<sup>2</sup>, or 60.9 m/s<sup>2</sup>, assuming that finite difference estimates using directly adjacent frames are used. *Burst noise* is produced when irregular events occur during the experiments. The tracking algorithm is built upon a set of assumptions, for

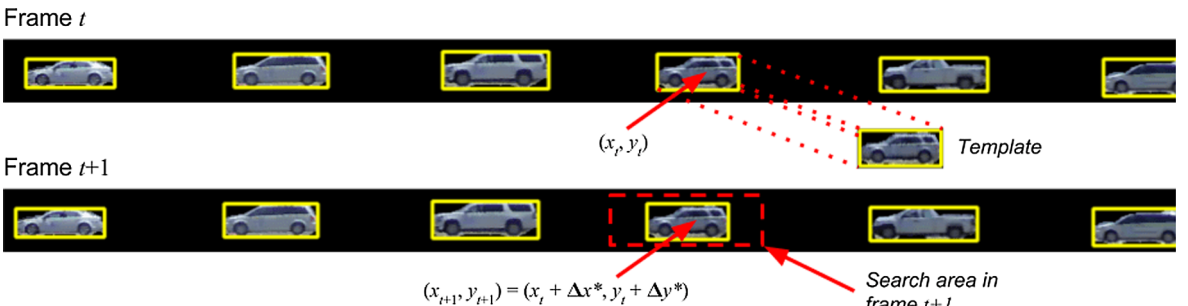


**Fig. 5.** Illustration of the tracking algorithm. For every vehicle in every frame, a small neighborhood is selected based on the location of that vehicle in the previous frame. The template is used to locate the current position of the vehicle via convolution.

example, the background subtraction step assumes stable lighting conditions. While those assumptions hold true most of the time, they are occasionally violated due to changing light conditions resulting from fast-moving clouds, or mirror-like reflectivity (i.e., specularity) of the vehicle paint. In these cases, one may observe burst noise in the raw vehicle trajectories.

To reduce the noise described above, a fourth-order weighted B-spline smoother is applied to reconstructed trajectories, which is able to substantially reduce the noise (Dierckx, 1982; Schumaker and Dierckx, 1994). The choice of a fourth-order B-spline allows for smoothness in the acceleration estimates of the vehicle trajectories. Concretely, the spline smoother uses a weighted square loss function, where splines are connected on the boundaries under  $C_3$  continuity. The weights are chosen such that acceleration estimates obtained from the second derivative of the B-splines are observed to be within physically reasonable bounds. Additionally, a parameter called *tolerance* (precisely, a limit on the sum of the absolute error between the data points and the spline over an interval) is used to control the length of every individual fitting window. Because a fourth-order spline is uniquely defined by five points, fitting error will likely arise if more than five points are given. Very commonly, such fitting error increases with the length of fitting window. Therefore, one can implicitly control window length by specifying a tolerance value such that the window is as long as possible under the constraint that the fitting error does not exceed the tolerance. The influence of the tolerance parameter on the accuracy of the trajectories is explored in detail in the Section 4.4. For a in-depth explanation of the spline smoother, please refer to the Section 5 of the work by Dierckx (1982) and the chapter 5.3 nu Schumaker and Dierckx (1994).

#### 4. Validation

The tracking algorithm described in Section 3 is validated both in terms of positional accuracy and in terms of velocity accuracy. Position estimates are compared with a manually labeled dataset, while the velocity data are validated by comparing to high-precision velocity data recorded on the highly instrumented University of Arizona *Cognitive and Autonomous Test Vehicle* (CAT Vehicle), which is vehicle number 20 in each experiment. Due to the lack of validation datasets for these measurements, only the distribution of vehicle accelerations and fuel rate are also presented. Finally, the choice of hyperparameter *tolerance* in the spline smoother is validated through a parameter sweeping scheme.

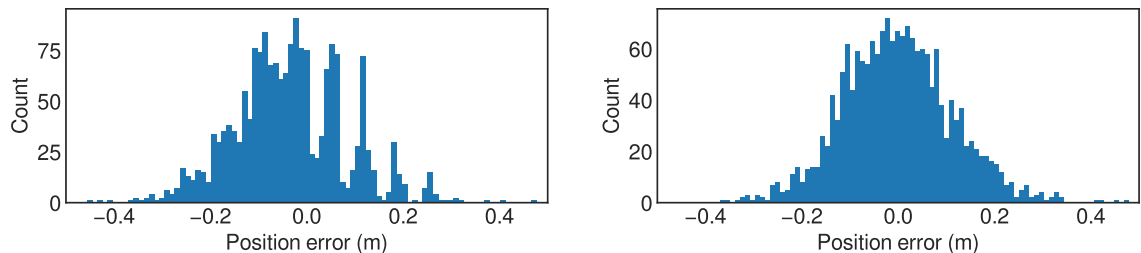
##### 4.1. Position accuracy

We compare the positions estimated from the image processing algorithm with manually labelled position data. Manual labels are generated through three human annotators using an online annotation tool, *LabelMe* (Russell et al., 2007). The annotators were asked to label the rear bumper location of vehicle 19 and the front bumper location of vehicle 20. One annotator labeled frames at a framerate of 3 Hz, for a total of 900 frames (five minutes) of Experiment A. Two additional annotators were instructed to independently label the first 30 s of the experiment at the same frame rate, so that the inter-annotator agreement can be computed for the three annotators. The sample standard deviation of the position labels is 0.05 m (about  $\frac{3}{4}$  pixels). Consequently the human annotation data can be used as a reasonable proxy of the *true* position of each vehicle.

The position data extracted from the camera are compared on the 900 frame dataset using both the raw and the smoothed camera trajectory data of vehicle 19 and 20. We treat the human annotated position estimates as the true position of the vehicle, from which error residuals and the standard deviation of the error distribution can be computed. The average error of the raw camera position estimates is  $-0.04$  m, and the standard deviation of the errors is 0.12 m. The average error of the smoothed camera trajectory is less than 0.002 m, and the errors have a standard deviation of 0.11 m. The error distributions of the raw and noise-reduced position estimates are shown in Fig. 6.

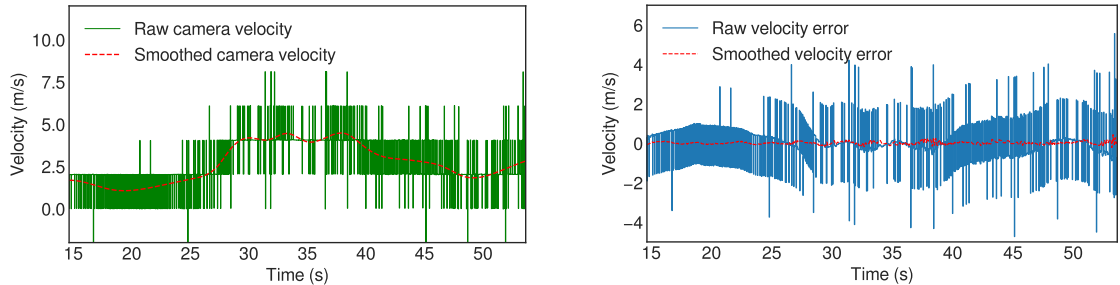
##### 4.2. Velocity accuracy

The accuracy of the smoothed camera velocity estimate is compared to the velocity recorded from an odometry sensor on vehicle 20 (the highly instrumented CAT Vehicle) in Experiment A. In the following discussion, we treat the odometry data from the CAT



(a) Distribution of the raw position errors with human-labeled positions taken as the true positions.  
(b) Distribution of the smoothed position errors with human-labeled positions taken as the true positions.

**Fig. 6.** Results of validation analysis on the position measurements in Experiment A.



(a) Comparison of velocity signals for vehicle 20 in Experiment A. The raw camera speed signal (green), quantized into integer multiples of 2.03 m/s oscillates around the smoothed camera velocity signal (red).

(b) Validation of velocity signals for vehicle 20 in Experiment A. Here the odometry velocity signal is selected as the reference. The difference between raw camera velocity signal and the reference is shown in blue, while the difference between smoothed velocity signal and the reference displayed in red.

**Fig. 7.** Analysis on B-spline smoothing for noise reduction. The time series plot shows the effects of the B-spline smoother. The residual plot illustrates that the noise reduction method significantly improves the data quality.

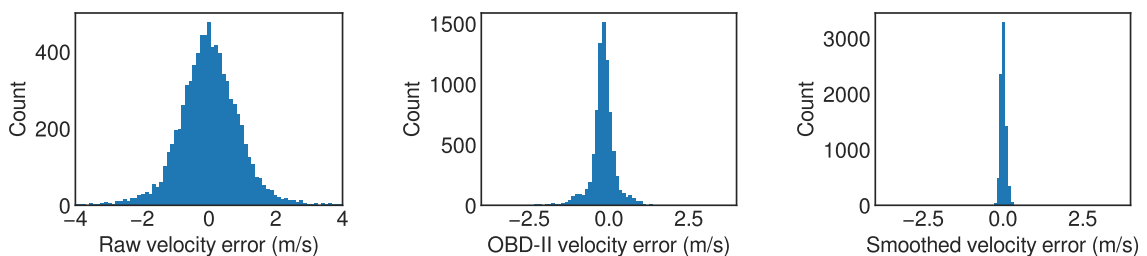
Vehicle as the true velocity signal from which errors are computed. We also compare the velocity recorded directly from the ScanTool OBDLink LX OBD-II scanner installed on all vehicles in the experiment (including the CAT Vehicle). Since the odometry-based velocity readings are recorded at 20 Hz, the 30 Hz camera data are downsampled from 30 Hz to 20 Hz for point by point comparison.

The difference between the raw camera signal and the smoothed camera signal for Experiment A is illustrated in Fig. 7a, while the accuracy of the raw and smoothed camera velocity is shown in Fig. 7b. In Fig. 7a, the raw camera velocity contains clear quantization errors with a step size of about 2.03 m/s, while the smoothed camera velocity is free of the quantization errors. Irregularly large estimates, or burst noises, in the raw camera velocity such as 8.12 m/s and -2.03 m/s are also removed in the smoothed data. As evident in Fig. 7b, the noise reduction technique converts the original noisy measurements to one that is one to two orders of magnitude closer to the odometry velocity.

In Fig. 8, the error distributions of the raw camera velocity, the OBD-II recorded velocity, and the smoothed camera velocity for vehicle 20 in Experiment A are shown. The smoothed camera velocity error distribution has a standard deviation (0.09 m/s) that is an order of magnitude smaller than the raw camera data (1.17 m/s), and it is also smaller than the OBD-II velocity error standard deviation (0.37 m/s). The surprising finding that the camera speeds are more precise is due to the (undocumented) internal processing of the OBD-II signal that occurs either on the vehicle or in the OBD-II scanner. From Fig. 9, we observe that the OBD-II recorded velocity is also quantized, and appears to hold the value of the recorded velocity constant over several seconds. This leads to larger errors than the smoothed camera velocity data.

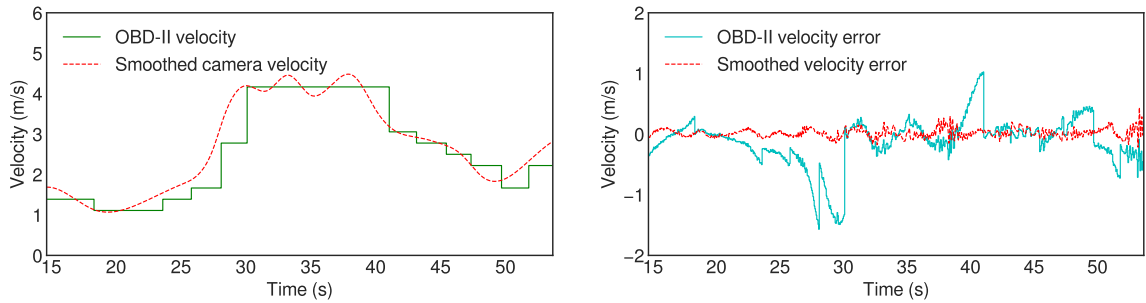
#### 4.3. Acceleration and fuel rate distribution

Due to the lack of other reliable measures against which the collected data can be validated, we are only able to show that the distribution of the accelerations and fuel rate data are physically plausible (e.g., the accelerations lie within the bounds of the physical performance limits of the vehicles). The distribution of acceleration measurements for all vehicles in Experiment A is shown in Fig. 10a, and the distribution of fuel rate measurements is shown in Fig. 10b. For common commercial vehicles, the magnitude of



(a) Distribution of difference between raw velocity and odometry velocity. (b) Distribution of difference between OBD-II velocity and odometry. (c) Distribution of difference between smoothed camera velocity and odometry velocity.

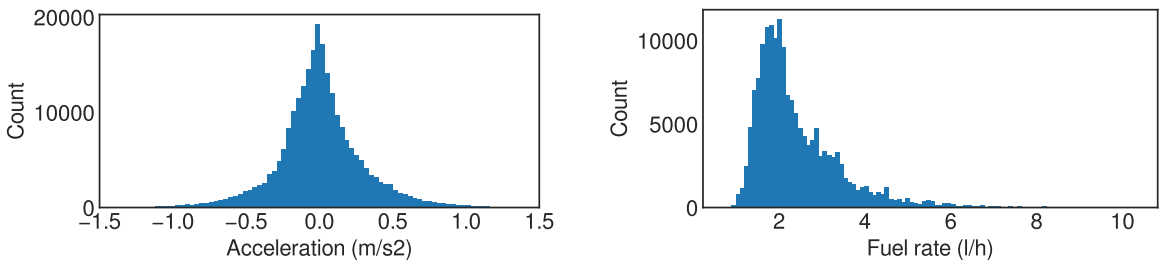
**Fig. 8.** Results of validation analysis on the speed measurements in Experiment A.



(a) Comparison of velocity signals for vehicle 20 in Experiment A. The OBD-II recorded speed signal (green) is quantized in time and space.

(b) Validation of velocity signals for vehicle 20 in Experiment A. Here the odometry velocity signal is selected as the reference. The difference between OBD-II velocity signal and the reference is shown in blue, while the difference between the smoothed velocity signal and the reference displayed in red.

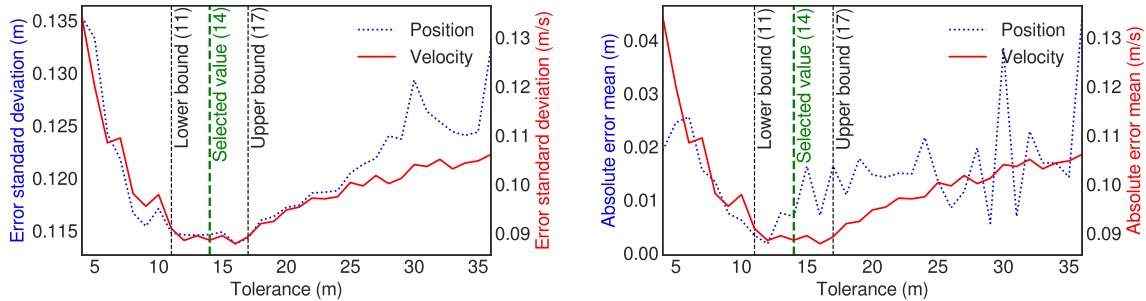
**Fig. 9.** Comparison between smoothed camera velocity data and OBD-II velocity data.



(a) Distribution of acceleration measurements.

(b) Distribution of fuel consumption rate measurements.

**Fig. 10.** Distributions of acceleration and fuel rate measurements in Experiment A.



(a) Error standard deviations as a function of the tolerance parameter used in B-spline smoothing.

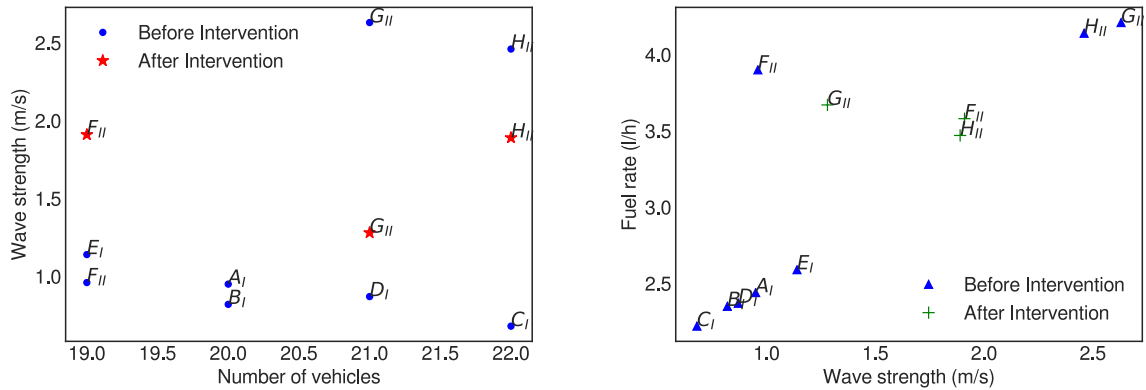
(b) Absolute error mean as a function of the tolerance parameter used in B-spline smoothing.

**Fig. 11.** Results of parameter tuning using the position labels and odometry measurements in Experiment A.

acceleration is less than 5 m/s<sup>2</sup> and the limit of fuel rate less than 25 l/h (Mehar et al., 2013; Administration, 2012). The collected dataset is shown to comply with these limits. In fact, the magnitude of acceleration rarely exceeds 1.5 m/s<sup>2</sup>, and the fuel rate rarely exceeds 8 l/h. The distributions of acceleration and fuel rate for the other experiments are similar to those of Experiment A, and are collectively summarized in Table 2b.

#### 4.4. Noise reduction parameters selection

Note that the results presented above are not sensitive to the tolerance parameter of the B-spline smoother. Fig. 11a shows the result of a sensitivity analysis, which illustrates that any tolerance value between 11 m and 17 m produces small error standard



(a) Wave strength as a function of the number of vehicles on the circular track showing: (i) instruction II on average generates stronger waves (measured by velocity standard deviation) than instruction I; and (ii) generally decreasing wave strength with increasing vehicle density for instruction I.

(b) Fuel rate as a function of wave strength indicating that when stronger traffic waves (greater velocity standard deviation) are present, vehicles consume more fuel.

**Fig. 12.** Summary of experiments depicting: (i) a general decreasing trend in wave strength as number of vehicles on the track increases for instruction I, and increasing wave strength with number of vehicles for instruction II, (ii) on average instruction II generates stronger waves (greater velocity standard deviation) than instruction I, and (iii) an observed increase in fuel rate with wave strength. \*The intervention in F was to slow down the traffic as opposed to maintain a constant speed in G and H. Because wave was amplified after the intervention, Experiment F was ended very quickly due to safety concerns.

**Table 2**

Summary of validation analysis on velocity, acceleration and fuel rate data. The velocity error for  $v$  is defined to be the difference between the velocity measure of interest  $v$  and the odometry velocity readings  $v_{odo}$ , i.e.,  $v - v_{odo}$ . Velocity bias  $\pm$  one standard deviation are reported.

\*The abnormal zero fuel rate readings recorded from vehicle 15 at the start of experiment A are excluded from the calculation.

Exp. no.	Raw velocity error (m/s)	OBD-II velocity error (m/s)	Smoothed velocity error (m/s)
A	$0.02 \pm 1.17$	$0.18 \pm 0.37$	$0.02 \pm 0.09$
B	$0.02 \pm 0.65$	$-0.18 \pm 0.32$	$0.02 \pm 0.08$
C	$0.03 \pm 0.62$	$-0.16 \pm 0.47$	$0.03 \pm 0.09$
D	$0.03 \pm 0.64$	$-0.17 \pm 0.28$	$0.03 \pm 0.11$
E	$0.02 \pm 0.61$	$-0.17 \pm 0.45$	$0.02 \pm 0.09$
F	$0.01 \pm 0.61$	$-0.23 \pm 0.34$	$0.01 \pm 0.11$
G	$0.01 \pm 0.61$	$-0.21 \pm 0.82$	$0.01 \pm 0.09$
H	$0.02 \pm 0.61$	$-0.20 \pm 0.57$	$0.02 \pm 0.08$

Exp. no.	Acceleration (m/s <sup>2</sup> )	Fuel rate (l/h)
A	$-3.17 \text{--} 1.79$	$0.71^* \text{--} 10.34$
B	$-1.78 \text{--} 2.33$	$0.89 \text{--} 09.38$
C	$-1.70 \text{--} 1.65$	$0.90 \text{--} 12.71$
D	$-2.22 \text{--} 1.98$	$0.77 \text{--} 13.65$
E	$-2.46 \text{--} 1.85$	$0.88 \text{--} 15.65$
F	$-3.65 \text{--} 3.50$	$0.76 \text{--} 22.12$
G	$-5.35 \text{--} 4.19$	$0.88 \text{--} 23.67$
H	$-4.45 \text{--} 4.05$	$0.86 \text{--} 23.45$

deviations in position data and velocity data. Fig. 11b indicates that the estimation bias in the position and velocity data are also minimized when the tolerance is between 11 m and 17 m. Consequently the tolerance parameter is set to be 14 m, which lies in the center of the optimal interval. Recall that the tolerance controls the cumulative error between the raw data and the B-spline, and indirectly controls the window (number of points fit with a single spline). When the tolerance is set to 14 m, the window typically contains hundreds or thousands of points.

Moreover, it is shown in Table 2 that the specific choice of the smoother parameter in Experiment A generalizes well to the other experiments. Specifically, we apply the optimal smoother parameter from experiment A to the remaining experiments, which were not used to determine the optimal parameter. Under the threshold choice of 14 m, the maximum (over all tests) mean error is 0.03 m/s with a standard deviation of 0.11 m/s of smoothed velocity error mean is 0.02 m/s, and the maximum ranges of smoothed velocity

**Table 3**

Summary of experiments conducted. Instruction I is to “*safely follow the vehicle in front as if in rush hour traffic*”, while instructions II is to “*place an emphasis on closing the gap the vehicle in front*.” In Experiment F, vehicle speeds were substantially higher than in the previous experiments so the driver of vehicle 20 was instructed to intervened by reducing the speed out of an abundance of caution. This was not intended to produce a smooth driving profile and actually increased the velocity standard deviation. Contrarily, in Experiments G, and H, the driver of vehicle 20 was intervened by an instruction to maintain a constant speed.  $\bar{v}$  is the average velocity,  $\sigma_v$  is the velocity standard deviation,  $\bar{r}$  is the average fuel rate, and  $\sigma_r$  is the fuel rate standard deviation.

Exp. no.	No. of vehicles	Instruction	$\bar{v} \pm \sigma_v$ before intervention (m/s)	$\bar{v} \pm \sigma_v$ after intervention (m/s)	$\bar{r} \pm \sigma_r$ before intervention (l/h/veh)	$\bar{r} \pm \sigma_r$ after intervention (l/h/veh)
A	20	I	$3.11 \pm 0.80$	n/a	$2.46 \pm 1.07$	n/a
B	20	I	$2.81 \pm 0.69$	n/a	$2.36 \pm 0.92$	n/a
C	22	I	$2.37 \pm 0.55$	n/a	$2.23 \pm 0.80$	n/a
D	21	I	$3.15 \pm 0.70$	n/a	$2.51 \pm 1.04$	n/a
E	19	I	$3.88 \pm 0.91$	n/a	$2.62 \pm 1.21$	n/a
F	19	II	$7.68 \pm 0.96$	$5.79 \pm 1.91$	$3.90 \pm 2.34$	$3.58 \pm 2.63$
G	21	II	$5.27 \pm 2.63$	$5.81 \pm 1.28$	$4.21 \pm 3.28$	$3.67 \pm 2.66$
H	22	II	$5.07 \pm 2.46$	$4.51 \pm 1.89$	$4.14 \pm 3.04$	$3.47 \pm 2.60$

error standard deviation is 0.03 m/s. Therefore the selected smoother parameters generalize well to other experiments and the high quality velocity estimates are not an artifact of overfitting the tolerance parameter on a single dataset.

#### 4.5. Data anomalies

Although the data collected from the experiments presented in this article are largely complete, there are a few anomalies that must be noted. These take the form of missing or erroneous measurements in the OBD-II data.

Concretely, the OBD-II fuel rate data (l/h) contain missing entries, zero readings, and an inconsistency in sampling rate. OBD-II data are missing from the following vehicles: Experiment D, vehicles 5 and 6; Experiment E, vehicle 3; Experiment F, vehicle 17; Experiment H, vehicle 4. Zero fuel rate readings are recorded for vehicle 15 in Experiment A for the first four seconds of the experiment. These missing data entries and zero readings are the result of operational errors with the OBD-II scanners during the experiment. Additionally, while the experiments are designed to collect OBD-II data at the maximum sampling rate of 20 Hz, the OBD-II scanner in vehicle 19 collected data at 10 Hz for all experiments due to an incorrect setting in the OBD-II logger.

### 5. Datasets

A summary of the data collected is first provided in [Table 3](#). Each experiment is then described with details, and followed next by a qualitative discussion of the experiment results. For a visual presentation of the data, please refer to [Fig. A.1](#) through [Fig. A.8](#) in the Appendix.

#### 5.1. Summary statistics

In [Table 3](#), the experiments are compared with respect to a number of quantitative measures.

To quantify the velocity variability (which is used as a measure of the wave strength), the velocity standard deviation for critical intervals in each test is presented. Precisely, the wave strength is quantified as the standard deviation of the  $m$  velocity measurements (per vehicle) from  $n$  vehicles over a time interval. Let  $v_t^i$  denote the  $t^{\text{th}}$  velocity measurement from vehicle  $i$ . The velocity standard deviation is computed as

$$\sigma_v = \left( \frac{1}{mn - 1} \sum_{t=1}^m \sum_{i=1}^n (v_t^i - \bar{v})^2 \right)^{\frac{1}{2}}, \quad (6)$$

where  $\bar{v}$  is the average velocity defined by:

$$\bar{v} = \frac{1}{mn} \sum_{t=1}^m \sum_{i=1}^n v_t^i. \quad (7)$$

Similarly, the average fuel rate  $\bar{r}$  and fuel rate standard deviation  $\sigma_r$  is also computed for each test.

For experiments A-E, the quantities are computed over the full experiment duration minus an initial period where the vehicles were accelerating from rest. In Experiments F-H, a single vehicle was commanded to reduce the speed (Experiment F) or to maintain a target speed (G and H). In these tests, the relevant quantities are computed both prior to the intervention and after the intervention.

## 5.2. Experiment descriptions

In Experiment A, 20 vehicles were deployed on the 260 m track, and instruction I was given to the drivers. The vehicle trajectories are shown in Fig. A.1, where small traffic waves are observed. The average speed was 3.11 m/s with a velocity standard deviation of 0.80 m/s, and the average fuel rate was measured to be 2.46 l/h/veh. The experiment ended after 416 s.

Experiment B was conducted with the same vehicle density and instruction as Experiment A. The resulting traffic was slightly slower and less oscillatory than in Experiment A. The waves are shown in Fig. A.2, where the average speed was 2.81 m/s, velocity standard deviation was 0.69 m/s. The fuel rate in this experiment was 2.36 l/h/veh. This experiment ended after 442 s.

The vehicle density increased from 20 vehicles to 22 vehicles in Experiment C, while maintaining the same driver instruction as before. The resulting traffic was both slower and had lower velocity standard deviation than both Experiments A and B. The traffic in Experiment C (shown in Fig. A.3) had an average velocity of 2.37 m/s, and a velocity standard deviation of 0.55 m/s. The average fuel rate in this experiment was 2.23 l/h/veh, which was also lower than both Experiment A and B where the vehicle density was lower. The experiment ended after 388 s.

Experiment D conducted with 21 vehicles, and the average speed and velocity standard deviation increased with respect to experiment C. The average speed was 3.15 m/s, and the velocity standard deviation was 0.70 m/s. In this experiment, a higher fuel rate than in the previous experiment of 2.51 l/h/veh was observed. The resulting vehicle trajectories can be seen in Fig. A.4. The experiment ended after 480 s.

The last experiment conducted with instruction I was Experiment E. This experiment had the lowest vehicle density with 19 vehicles on the track. The result was faster moving traffic with stronger waves as seen in Fig. A.5. The average velocity in this experiment was 3.88 m/s and the velocity standard deviation was 0.91 m/s. This was the fastest and most oscillatory traffic observed when instruction I was used. This also resulted in Experiment E having the highest fuel rate of all experiments that used instruction I, with a fuel rate of 2.62 l/h/veh. The experiment ended after 333 s.

To contrast the effect on the development of traffic waves of the instructions given to drivers, Experiment F was also conducted with 19 vehicles on the track. However, different from Experiment E, in Experiment F, drivers were given instruction II. In this case, a larger velocity standard deviation was observed compared to the experiments in which instruction I was given, as seen in Fig. A.6. The average velocity over the first 59 s of the experiment was 7.68 m/s, nearly twice the velocity in any of the previous experiments. Due to the substantial speed increase, the driver of the CAT Vehicle (vehicle 20) was told via radio to slow down the traffic. The result of this was a slowdown of all vehicles on the track, as seen in Fig. A.6. The average velocity standard deviation over the first 59 s was 0.96 m/s and the fuel rate over the same interval was observed to be 3.90 l/h/veh. Since the slow-down intervention amplified strong stop-and-go wave, to avoid the wave be amplified beyond the safe range, the experiment was ended after only 175 s.

Experiment G was conducted with 21 vehicles on the track, using instruction II. The resulting traffic waves were larger than those in Experiment F, and significantly more pronounced than the oscillations observed in Experiments A through E. The average speed was 5.27 m/s (velocity standard deviation of 2.63 m/s) and the fuel rate was 4.21 l/h/veh over the first 312 s of the experiment. At this point, the driver of the CAT Vehicle was again instructed to drive with a constant speed, this time of 6.26 m/s (specifically, the command to drive at 14 mph was given, since a US vehicle was used). However, due to the limits in the precision of human driving behavior, this speed was not strictly maintained by the CAT Vehicle. After the intervention the velocity standard deviation decreased by more than a half to 1.36 m/s. This indicates that a single vehicle may be able to reduce the speed variability of the flow. This is seen in Fig. A.7. The experiment ended after 587 s.

To further explore the difference in wave development under instructions I and II, Experiment H was conducted with instruction II and 22 vehicles on the track. The average speed in the first 191 s of the experiment was 5.07 m/s, the velocity standard deviation was 2.46 m/s, and the average fuel rate was 4.14 l/h/veh. As with Experiment G compared to D, Experiment H compared to C had significantly larger waves, and a significantly higher fuel rate due to the change in the instructions. Again as in Experiment G, the driver of a single vehicle was instructed to maintain a constant after some time. In the case of Experiment H, this occurs twice: first after 191 s when the driver of the CAT Vehicle was instructed to drive at 5.36 m/s (12 mph), and after 411 s, when the driver of the CAT Vehicle was instructed to reduce the speed to 4.47 m/s (10 mph). The influence of this intervention on the vehicle speeds and vehicle trajectories is observed in Fig. A.8. The velocity standard deviation while the CAT Vehicle was intervening is lower than in the first portion of the experiment. Experiment H ended after 545 s.

Note that the interventions in Experiment G and H were different from the intervention in Experiment F. In Experiment F, the driver was instructed to slow down the traffic, while in Experiment G and H, the driver was instructed to maintain a constant velocity. This resulted the distinct effects of interventions as shown in Fig. 12a: The Experiment F intervention amplified the wave while the Experiment G and H interventions dampeden it.

## 5.3. Observations

The general trends observed in the data are outlined as follows: (i) the instructions given to drivers make a significant difference on the magnitude of waves; (ii) when instruction I was given, over the range of densities explored, lower density results in stronger waves (measured as the instantaneous velocity standard deviation of all vehicles averaged over the duration of the experiment); and (iii) stronger waves result in a higher fuel rate.

The velocity standard deviation depends strongly on the instructions given to the drivers. This is seen in Fig. 12a, where the blue

circles represent experiment runs in which drivers were given instruction I and instructed to, “follow the vehicle in front and drive as if you were in rush hour traffic,” while the red stars are trials where drivers were given instruction II and told to “place an emphasis on closing the gap with the vehicle in front.”

Compared to experiments with instruction I, on average stronger waves appeared in experiments with instruction II. This indicates that aggressive driving behavior will induce greater velocity variations, causing the traffic to exhibit speed oscillations.

In instruction I, the intensity of traffic waves observed also depends on the vehicle density. The relationship between the number of vehicles and the intensity of the waves as measured as velocity standard deviation is seen in Fig. 12a. This shows a general negative correlation between the number of vehicles on the track, and the intensity of the waves observed when instruction I is given.

The effect of traffic waves on the vehicle fuel rate is seen in Fig. 12b, where a clear increasing trend is observed between the velocity standard deviation and the average fuel rate. This result indicates that oscillatory traffic with a high velocity standard deviation is bad from a fuel rate standpoint.

## 6. Conclusion

This article describes a set of eight experiments in which 19–22 vehicles drive in a ring and traffic waves emerge. Trajectory data are extracted via an offline image processing algorithm that produces accurate trajectories. The produced trajectory data are very accurate: the mean position bias is less than 0.002 m with a small standard deviation of 0.11 m as compared to human-labeled data. The derived velocity estimates are also reliable: the mean velocity biased is only 0.02 m/s with a small standard deviation of 0.09 m/s. Additionally, each vehicle is instrumented with an OBD-II scanner to log the fuel rate throughout each experiment, providing a link between traffic waves and fuel consumption.

We believe that the produced trajectory and fuel rate data are an asset to the transportation research community. They directly support many types of empirical research including microscopic model calibration, studying driving behavior, fuel consumption modelling, and vehicle emission modelling. In the interest of research reproducibility and open access, we have made the data and the Python implementation of the tracking algorithms freely available online ([Wu, 2017](#)).

## Acknowledgements

This material is based upon work supported by the National Science Foundation under Grant No. CNS-1446715 (B.P.), CNS-1446690 (B.S.), CNS-1446435 (J.S.), and CNS-1446702 (D.W.). This research was supported by the Inria associated team “ModEling autonoMous vEhicles iN Traffic flOw (MEMENTO)”. The authors thank the University of Arizona Motor Pool in providing the vehicle fleet. They offer additional special thanks for the services of N. Emptage in carrying out the experiment logistics.

## Appendix A

First included in the appendix is the full verbal description of instruction I and II. The appendix also contains vehicle trajectories for all experiments presented in this article. Trajectory plots are independently colored by the corresponding spacing (to the rear bumper of the front vehicle), speed, acceleration, and fuel rate data. Lastly, the appendix includes specifications of each vehicle used in the experiments in [Table A.1](#).

### A.1. Driver instructions

Instruction I: Drive as you would if you were in rush hour traffic. Follow the vehicle ahead without falling behind. However, drive as safely as would on the road. Do not pass the car in front of you. Do not hit the car in front of you.

Instruction II: Drive as if you were in rush hour traffic. Follow the vehicle ahead without falling behind. Do not pass the car ahead. Do not hit the car ahead. Drive safely at all times. Do not tailgate. But put an emphasis on closing up to the vehicle ahead, if a gap starts opening up.

## A.2. Data visualizations

Figs. A.1, A.2, A.3, A.4, A.5, A.6, A.7, A.8.

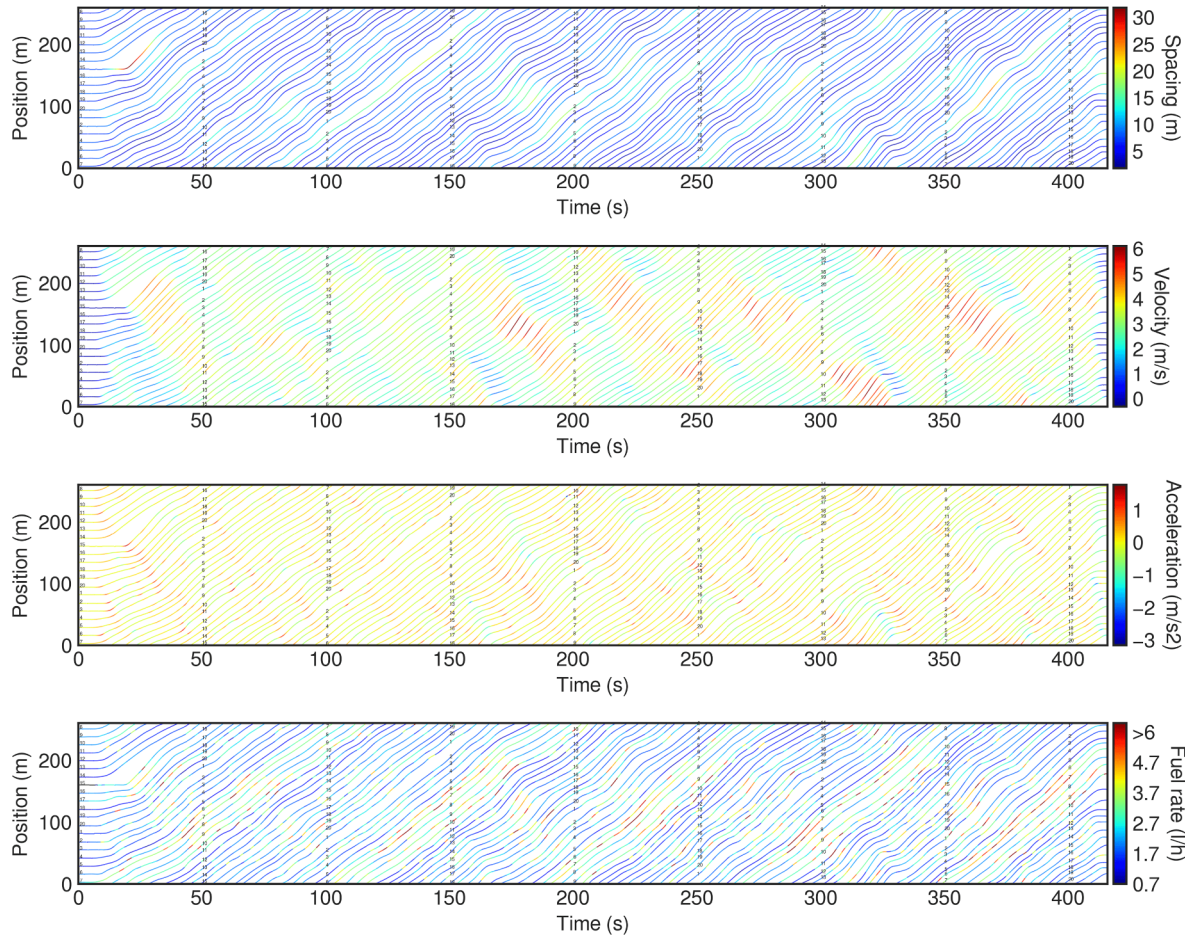


**Fig. A.1.** Visualization of Experiment A Data. Note that the color map fuel rate plot is capped at 6 l/h for enhanced visibility. A small fraction of measurements exceed 6 l/h, the maximum of which reaches 10.34 l/h. Black color indicates that no data are recorded. (For interpretation of the references to colour in this figure legend, the reader is referred to the web version of this article.)

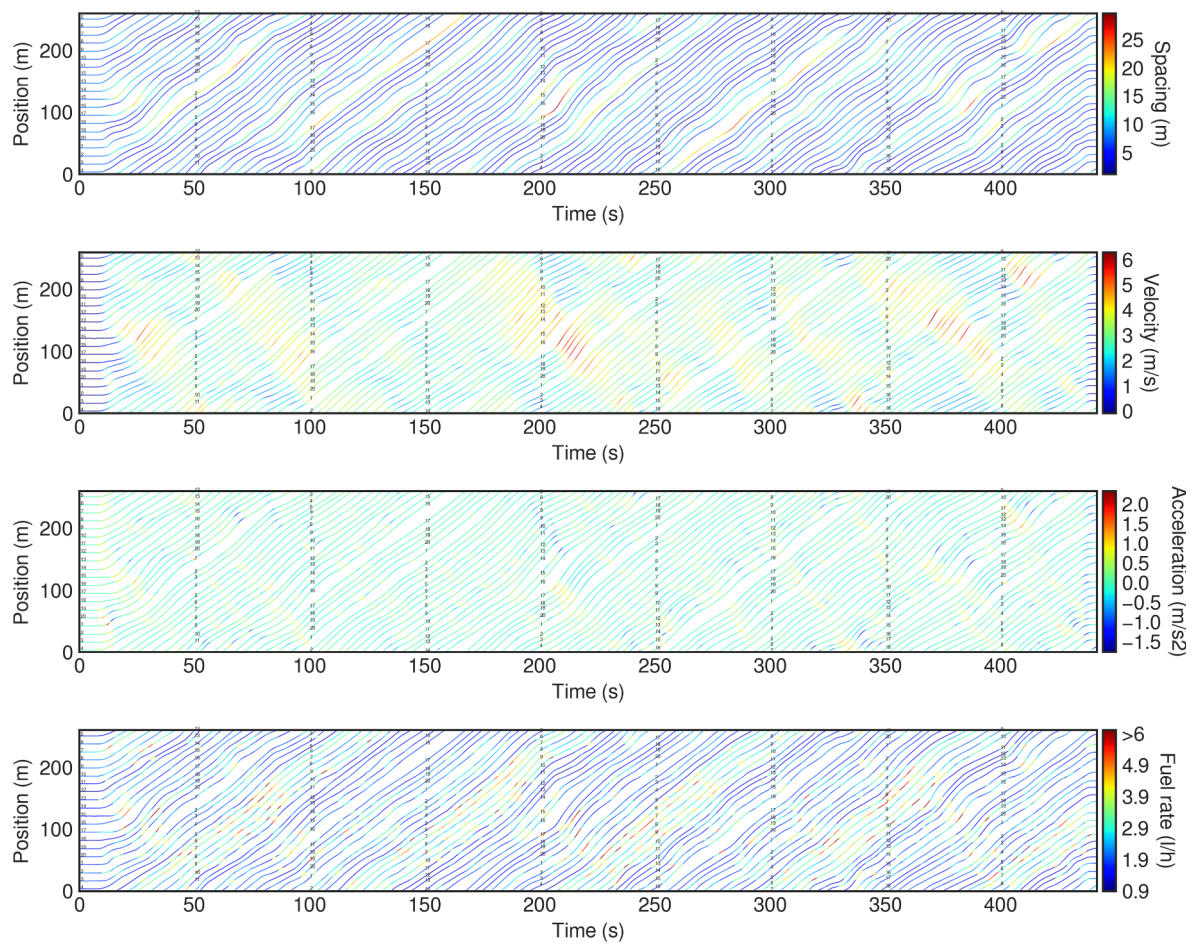


**Fig. A.2.** Visualization of Experiment B Data. Note that the color map fuel rate plot is capped at 6 l/h for enhanced visibility. A small fraction of measurements exceed 6 l/h, the maximum of which reaches 9.38 l/h. Black color indicates that no data are recorded. (For interpretation of the references to colour in this figure legend, the reader is referred to the web version of this article.)

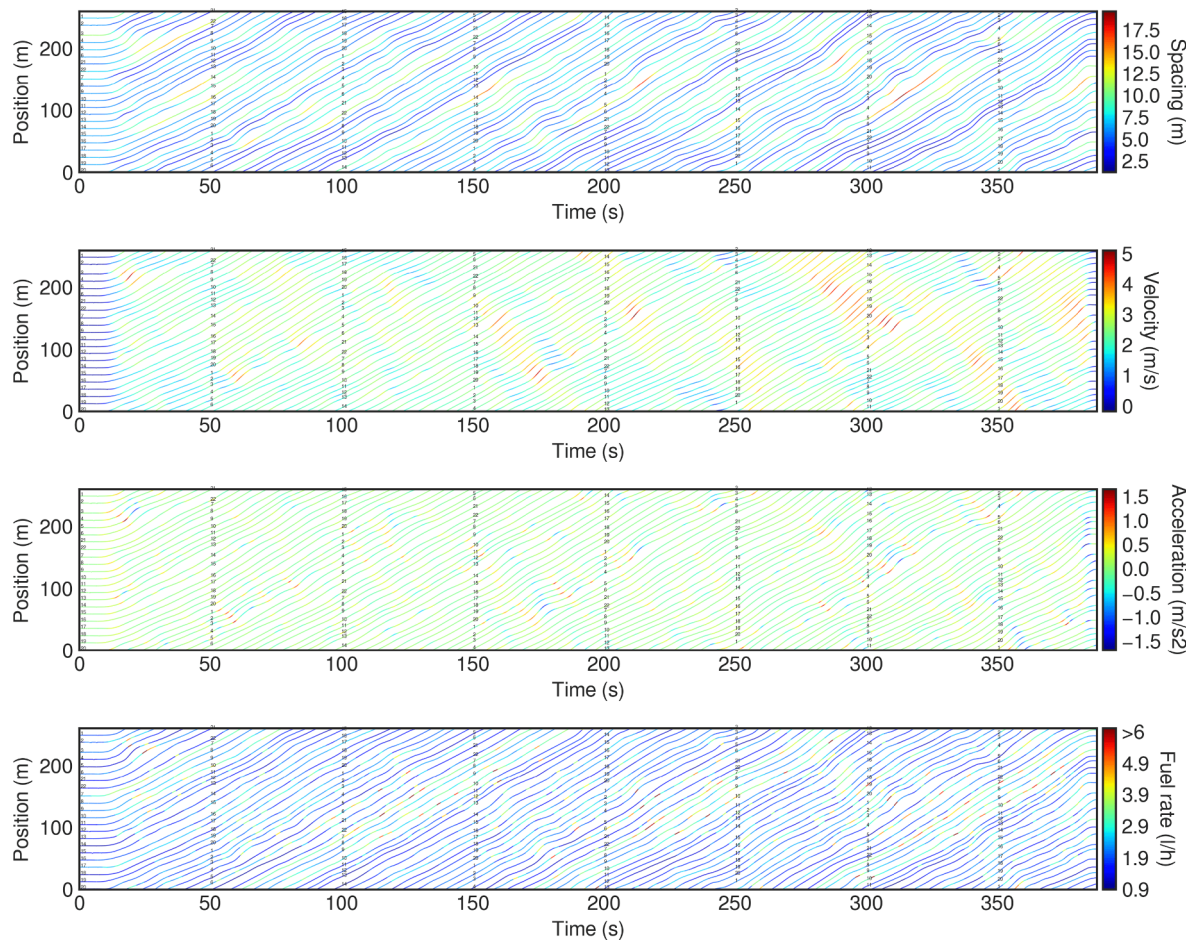


**Fig. A.3.** Visualization of Experiment C Data. Note that the color map fuel rate plot is capped at 6 l/h for enhanced visibility. A small fraction of measurements exceed 6 l/h, the maximum of which reaches 12.71 l/h. Black color indicates that no data are recorded. (For interpretation of the references to colour in this figure legend, the reader is referred to the web version of this article.)

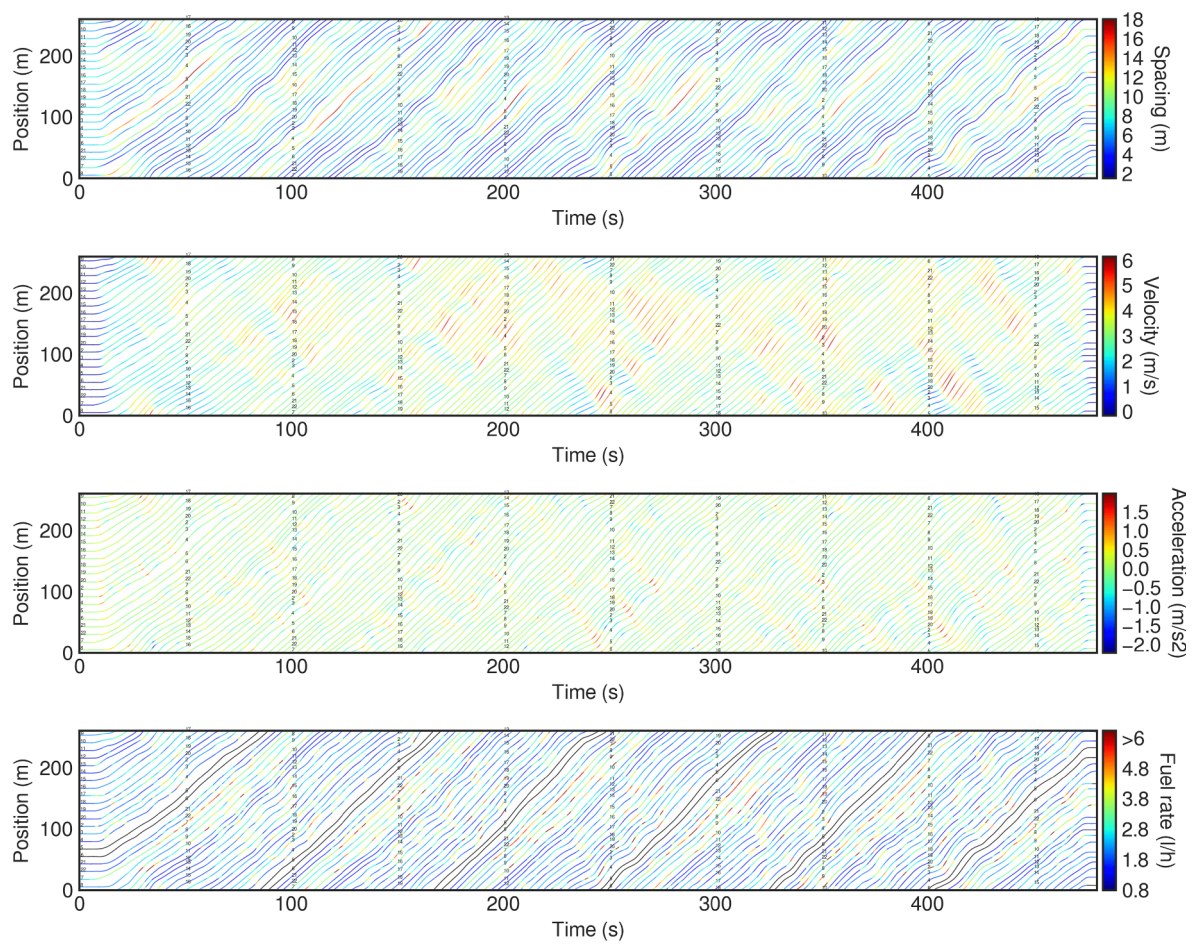


**Fig. A.4.** Visualization of Experiment D Data. Note that the color map fuel rate plot is capped at 6 l/h for enhanced visibility. A small fraction of measurements exceed 6 l/h, the maximum of which reaches 13.65 l/h. Black color indicates that no data are recorded. (For interpretation of the references to colour in this figure legend, the reader is referred to the web version of this article.)

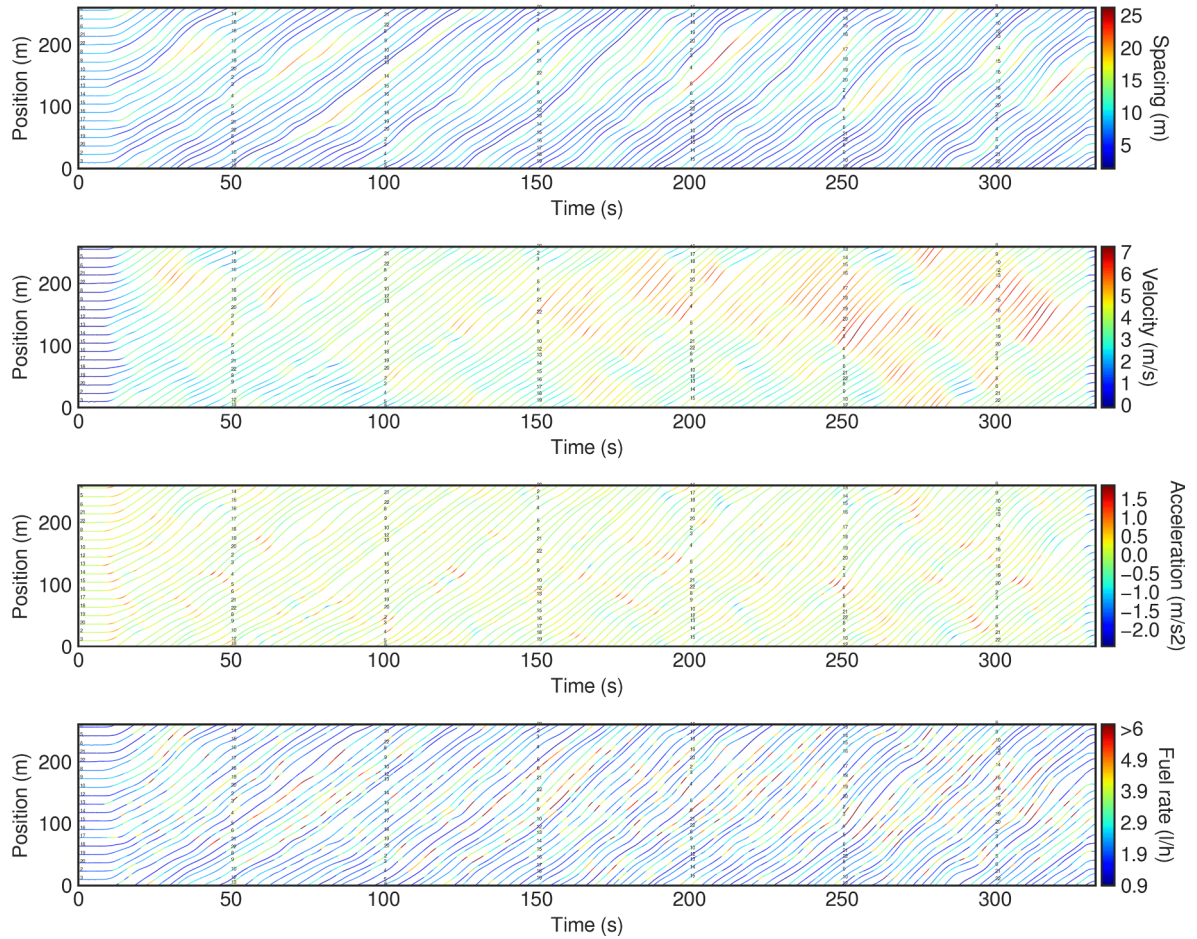


**Fig. A.5.** Visualization of Experiment E Data. Note that the color map fuel rate plot is capped at 6 l/h for enhanced visibility. A small fraction of measurements exceed 6 l/h, the maximum of which reaches 15.65 l/h. Black color indicates that no data are recorded. (For interpretation of the references to colour in this figure legend, the reader is referred to the web version of this article.)

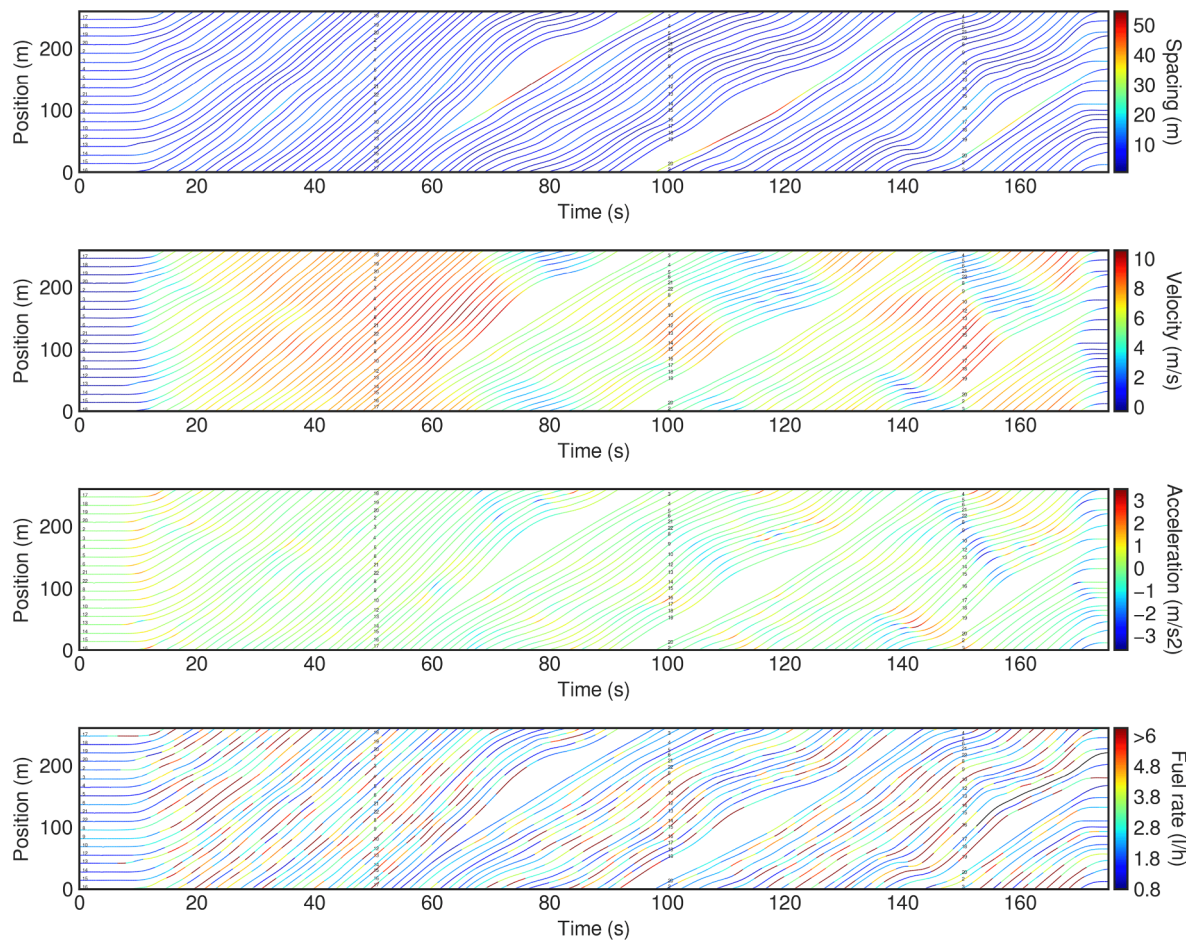


**Fig. A.6.** Visualization of Experiment F Data. Note that the color map fuel rate plot is capped at 6 l/h for enhanced visibility. A small fraction of measurements exceed 6 l/h, the maximum of which reaches 22.12 l/h. Black color indicates that no data are recorded. (For interpretation of the references to colour in this figure legend, the reader is referred to the web version of this article.)

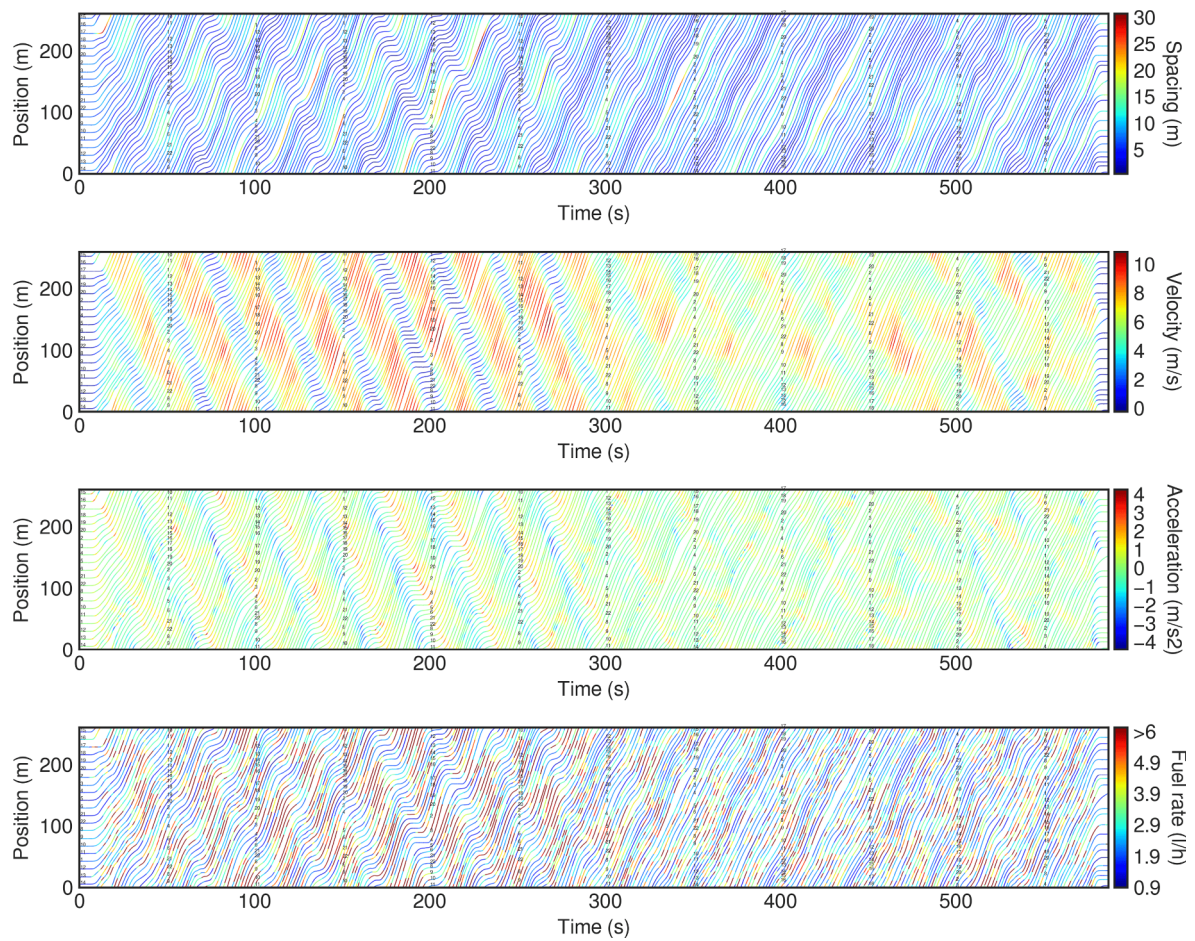


**Fig. A.7.** Visualization of Experiment G Data. Note that the color map fuel rate plot is capped at 6 l/h for enhanced visibility. A small fraction of measurements exceed 6 l/h, the maximum of which reaches 23.67 l/h. Black color indicates that no data are recorded. (For interpretation of the references to colour in this figure legend, the reader is referred to the web version of this article.)

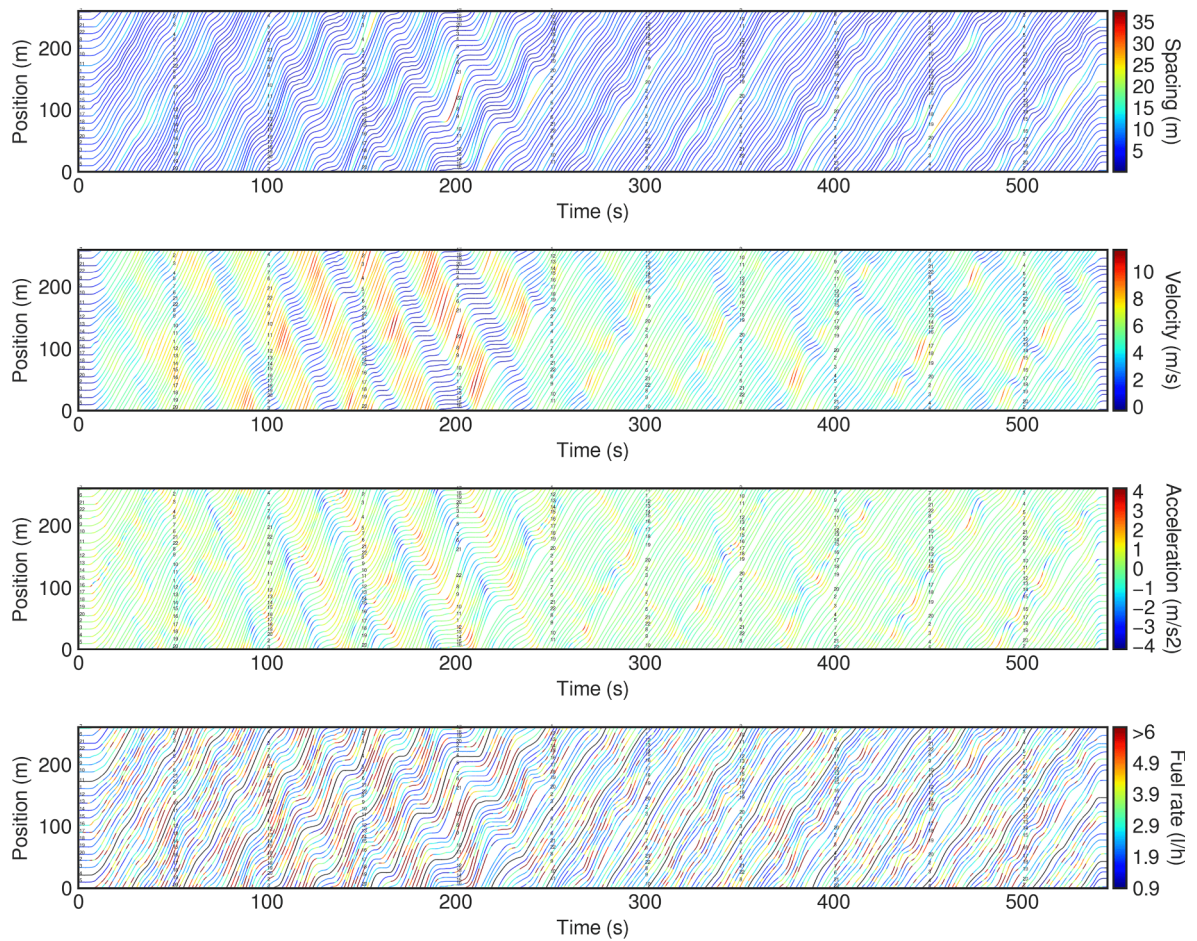


**Fig. A.8.** Visualization of Experiment H Data. Note that the color map fuel rate plot is capped at 6 l/h for enhanced visibility. A small fraction of measurements exceed 6 l/h, the maximum of which reaches 23.46 l/h. Black color indicates that no data are recorded. (For interpretation of the references to colour in this figure legend, the reader is referred to the web version of this article.)

### A.3. Vehicle specifications

**Table A.1.**

**Table A.1**

Specifications of vehicles in the experiments.

Veh. num.	Year	Make	Model	Length (m)	Consumption City (ℓ/100 km)	Consumption Hwy. (ℓ/100 km)
1	2013	Dodge	Grand Caravan	5.15	13.83	9.41
2	2013	Dodge	Grand Caravan	5.15	13.83	9.47
3	2012	Dodge	Grand Caravan	5.15	13.83	9.47
4	2012	Chevrolet	Malibu	4.87	10.69	7.13
5	2014	Dodge	Grand Caravan	5.15	13.83	9.41
6	2015	Chevrolet	Suburban	5.69	14.71	10.22
7	2016	Chevrolet	Express 2500	5.69	21.38	14.70
8	2016	Dodge	Grand Caravan	5.15	13.83	9.41
9	2013	Chevrolet	Silverado	5.22	15.67	10.68
10	2014	Chevrolet	Silverado	5.21	13.07	9.80
11	2014	Chevrolet	Malibu	4.86	9.41	6.53
12	2014	Chevrolet	Malibu	4.86	9.41	6.53
13	2016	Chevrolet	Malibu Limited	4.86	9.80	6.92
14	2015	Chevrolet	Malibu	4.92	9.41	6.53
15	2012	Chevrolet	Malibu	4.87	10.70	7.13
16	2012	Dodge	Grand Caravan	5.15	13.83	9.41
17	2013	Chevrolet	Impala	5.09	13.07	7.84
18	2015	Chevrolet	Malibu	4.86	9.47	6.53
19	2016	Chevrolet	Suburban	5.70	14.71	10.22
20	2009	Ford	Escape Hybrid	4.44	6.92	7.84
21	2014	Chevrolet	Malibu	4.86	9.41	6.53
22	2012	Chevrolet	Malibu	4.87	10.70	7.13

### A.4. Experiment fleet

**Table A.2.**

**Table A.2**

Vehicles used for each experiment. An  $\times$  appears if a vehicle was used for a given experiment. Each vehicle has a unique driver throughout the experiments.

Veh. num.	Exp. A	Exp. B	Exp. C	Exp. D	Exp. E	Exp. F	Exp. G	Exp. H
1	$\times$	$\times$	$\times$				$\times$	$\times$
2	$\times$							
3	$\times$							
4	$\times$							
5	$\times$							
6	$\times$							
7	$\times$	$\times$	$\times$	$\times$				
8	$\times$							
9	$\times$							
10	$\times$							
11	$\times$	$\times$	$\times$	$\times$				
12	$\times$							
13	$\times$							
14	$\times$							
15	$\times$							
16	$\times$							
17	$\times$							
18	$\times$							
19	$\times$							
20	$\times$							
21				$\times$	$\times$	$\times$	$\times$	$\times$
22				$\times$	$\times$	$\times$	$\times$	$\times$

## References

- Administration, U.E.I., 2012. Annual Energy Review.
- Aydos, C., Hengst, B., Uther, W., 2009. Kalman filter process models for urban vehicle tracking. In: Proceedings of the 12th IEEE International Conference on Intelligent Transportation Systems, pp. 1–8.
- Badenas, J., Pla, F., 1998. Applying computer vision techniques to traffic monitoring tasks. In: Lecture Notes in Computer Science Methodology and Tools in Knowledge-Based Systems, pp. 776–785.
- Bando, M., Hasebe, K., Nakayama, A., Shibata, A., Sugiyama, Y., 1995. Dynamical model of traffic congestion and numerical simulation. *Phys. Rev. E* 51 (2), 1035.
- Bar-Shalom, Y., Kirubarajan, T., Li, X.-R., 2007. Estimation with Applications to Tracking and Navigation. Wiley.
- Besselink, B., Johansson, K.H., 2017. String stability and a delay-based spacing policy for vehicle platoons subject to disturbances. Available from: arXiv:1702.01031.
- Blackman, S.S., Popoli, R., 1999. Design and analysis of modern tracking systems. Artech House.
- Bose, A., Ioannou, P.A., 2003. Analysis of traffic flow with mixed manual and semiautomated vehicles. *IEEE Trans. Intell. Transport. Syst.* 4 (4), 173–188.
- Buch, N., Velastin, S.A., Orwell, J., 2011. A review of computer vision techniques for the analysis of urban traffic. *IEEE Trans. Intell. Transport. Syst.* 12 (3), 920–939.
- Buehler, M., Iagnemma, K., Singh, S., 2009. The DARPA Urban Challenge: Autonomous Vehicles in City Traffic, vol. 56 Springer.
- Chandler, R.E., Herman, R., Montroll, E.W., 1958. Traffic dynamics: studies in car following. *Oper. Res.* 6 (2), 165–184.
- Coifman, B., 1997. Time space diagrams for thirteen shock waves. California Partners for Advanced Transit and Highways (PATH).
- Darbha, S., Rajagopal, K., 1999. Intelligent cruise control systems and traffic flow stability. *Transport. Res. Part C: Emerg. Technol.* 7 (6), 329–352.
- Davis, L.C., 2004. Effect of adaptive cruise control systems on traffic flow. *Phys. Rev. E* 69 (6), 066110.
- De Wit, C.C., Morbidi, F., Ojeda, L.L., Bélicot, I., Bellemain, P., 2015. Grenoble traffic lab: an experimental platform for advanced traffic monitoring and forecasting [applications of control]. *IEEE Control Syst.* 35 (3), 23–39.
- Dervisoglu, G., Gomes, G., Kwon, J., Horowitz, R., Varaiya, P., 2009. Automatic calibration of the fundamental diagram and empirical observations on capacity. In: Proceedings of the 88th Transportation Research Board Annual Meeting, vol. 15.
- Dervisoglu, G., Kurzhanskiy, A., Gomes, G., Horowitz, R., 2014. Macroscopic freeway model calibration with partially observed data, a case study. In: Proceedings of the American Control Conference, 2014. IEEE, pp. 3096–3103.
- Dierckx, P., 1982. Algorithms for smoothing data with periodic and parametric splines. *Comput. Graph. Image Process.* 20 (2), 171–184.
- Duong, D., Saccomanno, F., Hellings, B., 2010. Calibration of microscopic traffic model for simulating safety performance. In: Proceedings of the 89th Annual Meeting of the Transportation Research Board.
- Edelsbrunner, H., Seidel, R., 1986. Voronoi diagrams and arrangements. *Discr. Comput. Geom.* 1 (1), 25–44.
- Ester, M., Kriegel, H.-P., Sander, J., Xu, X., 1996. A density-based algorithm for discovering clusters in large spatial databases with noise. In: Proceedings of the Second International Conference on Knowledge Discovery and Data Mining. AAAI Press, pp. 226–231.
- Fang, Y., Shi, Z., Cao, J., 2014. Calibration of an interrupted traffic flow system using ngsim trajectory data sets. In: Proceedings of the 11th World Congress on Intelligent Control and Automation (WCICA). IEEE, pp. 4887–4892.
- Farneback, G., 2003. Two-frame motion estimation based on polynomial expansion. *Lect. Notes Comput. Sci.* 2749, 363–370.
- Federal Highway Administration, 2017. Next Generation Simulation (NGSIM). < <https://ops.fhwa.dot.gov/trafficanalysistools/ngsim.htm> > .
- Fenton, R.E., Mayhan, R.J., 1991. Automated highway studies at the Ohio State University—an overview. *IEEE Trans. Veh. Technol.* 40 (1), 100–113.
- Fitch, G.M., Soccilich, S.A., Guo, F., McClafferty, J., Fang, Y., Olson, R.L., Perez, M.A., Hanowski, R.J., Hankey, J.M., Dingus, T.A., 2013. The impact of hand-held and hands-free cell phone use on driving performance and safety-critical event risk. Technical report, Virginia Polytechnic Institute and State University.
- Forsyth, D., Ponce, J., 2015. Computer vision: a modern approach. Pearson.
- Foss, R.D., Goodwin, A.H., 2014. Distracted driver behaviors and distracting conditions among adolescent drivers: findings from a naturalistic driving study. *J. Adolescent Health* 54 (5), S50–S60.
- Gazis, D.C., Foote, R.S., 1969. Surveillance and control of tunnel traffic by an on-line digital computer. *Transport. Sci.* 3 (3), 255–275.
- Gazis, D.C., Herman, R., Potts, R.B., 1959. Car-following theory of steady-state traffic flow. *Oper. Res.* 7 (4), 499–505.
- Gerlach, D.L., Huber, M.J., 1975. Traffic flow theory.
- Greenshields, B., 1934. The photographic method of studying traffic behavior. In: Highway Research Board Proceedings, vol. 13.
- Guérin, M., Billot, R., El Faouzi, N.-E., Monteil, J., Armetta, F., Hassas, S., 2016. How to assess the benefits of connected vehicles? A simulation framework for the design of cooperative traffic management strategies. *Transport. Res. Part C: Emerg. Technol.* 67, 266–279.
- Helbing, D., Tilch, B., 1998. Generalized force model of traffic dynamics. *Phys. Rev. E* 58 (1), 133.
- Herman, R., Potts, R.B., 1959. Single lane traffic theory and experiment.
- Herrera, J.C., Work, D.B., Herring, R., Ban, X.J., Jacobson, Q., Bayen, A.M., 2010. Evaluation of traffic data obtained via GPS-enabled mobile phones: the Mobile Century field experiment. *Transport. Res. Part C: Emerg. Technol.* 18 (4), 568–583.
- Hoogendoorn, S., Ossen, S., Schreuder, M., 2006. Empirics of multianticipative car-following behavior. *Transport. Res. Rec.: J. Transport. Res. Board* (1965), 112–120.
- Huang, Y.-X., Jiang, R., Zhang, H.M., Hu, M.-B., Tian, J.-F., Jia, B., Gao, Z.-Y., 2018. Experimental study and modeling of car-following behavior under high speed situation. *Transport. Res. Part C: Emerg. Technol.* 97, 194–215.
- Hueper, J., Dervisoglu, G., Muralidharan, A., Gomes, G., Horowitz, R., Varaiya, P., 2009. Macroscopic modeling and simulation of freeway traffic flow. *IFAC Proc.* 42 (15), 112–116.
- Hwasoo, Y., Skabardonis, A., 2009. Understanding stop-and-go traffic in view of asymmetric traffic theory. In: Transportation and Traffic Theory 2009: Golden Jubilee. Springer, pp. 99–115.
- Ioannou, P., Xu, Z., Eckert, S., Clemons, D., Sieja, T., 1993. Intelligent cruise control: theory and experiment. In: Proceedings of the 32nd IEEE Conference on Decision and Control. IEEE, pp. 1885–1890.
- Jiang, R., Hu, M.-B., Zhang, H.M., Gao, Z.-Y., Jia, B., Wu, Q.-S., 2015. On some experimental features of car-following behavior and how to model them. *Transport. Res. Part B: Methodol.* 80, 338–354.
- Jiang, R., Hu, M.-B., Zhang, H.M., Gao, Z.-Y., Jia, B., Wu, Q.-S., Wang, B., Yang, M., 2014. Traffic experiment reveals the nature of car-following. *PLOS ONE* 9 (4), 1–9.
- Jiang, R., Jin, C.-J., Zhang, H.M., Huang, Y.-X., Tian, J.-F., Wang, W., Hu, M.-B., Wang, H., Jia, B., 2017. Experimental and empirical investigations of traffic flow instability. *Transport. Res. Proc.* 23, 157–173.
- Kastrinaki, V., Zervakis, M., Kalaitzakis, K., 2003. A survey of video processing techniques for traffic applications. *Image Vis. Comput.* 21 (4), 359–381.
- Kesting, A., Treiber, M., 2008a. Calibrating car-following models by using trajectory data: methodological study. *Transport. Res. Rec.: J. Transport. Res. Board* 2088, 148–156.
- Kesting, A., Treiber, M., 2008b. Calibrating car-following models by using trajectory data: methodological study. *Transport. Res. Rec.: J. Transport. Res. Board* 2088, 148–156.
- Levine, W., Athans, M., 1966. On the optimal error regulation of a string of moving vehicles. *IEEE Trans. Autom. Control* 11 (3), 355–361.
- Lipton, A.J., Fujiyoshi, H., Patil, R.S., 1998. Moving target classification and tracking from real-time video. In: Proceedings of the Fourth IEEE Workshop on Applications of Computer Vision. IEEE, pp. 8–14.
- Liu, H., Sun, F., He, K., 2007. Symmetry-aided particle filter for vehicle tracking. In: Proceedings 2007 IEEE International Conference on Robotics and Automation, pp. 4633–4638.
- Liu, W., Anguelov, D., Erhan, D., Szegedy, C., Reed, S., Fu, C.-Y., Berg, A.C., 2016. Ssd: single shot multibox detector. In: European Conference on Computer Vision. Springer, pp. 21–37.

- Lu, X.-Y., Varaiya, P., Horowitz, R., 2009. Fundamental diagram modelling and analysis based ngsim data. *IFAC Proc.* 42 (15), 367–374.
- May, A.D., Cayford, R., Coifman, B., Merritt, G., 2003. Loop detector data collection and travel time measurement in the berkeley highway laboratory. California Partners for Advanced Transit and Highways (PATH).
- McGregor, G., 2013. On Microscopic Traffic Models, Intersections and Fundamental Diagrams. PhD thesis, University of Victoria.
- Mehar, A., Chandra, S., Velmurugan, S., 2013. Speed and acceleration characteristics of different types of vehicles on multi-lane highways. *Euro. Transport* 55, 1825–3997.
- Milan, A., Rezatofighi, S.H., Dick, A., Reid, I., Schindler, K., 2016. Online multi-target tracking using recurrent neural networks.
- Montanino, M., Punzo, V., 2015. Trajectory data reconstruction and simulation-based validation against macroscopic traffic patterns. *Transport. Res. Part B: Methodol.* 80, 82–106.
- Montgomery, J., Kusano, K.D., Gabler, H.C., 2014. Age and gender differences in time to collision at braking from the 100-car naturalistic driving study. *Traffic Inj. Prevent.* 15 (sup1), S15–S20.
- Nahm, N.E., Trivedi, A.N., 1973. Recursive estimation of traffic variables: section density and average speed. *Transport. Sci.* 7 (3), 269–286.
- Nakayama, A., Fukui, M., Kikuchi, M., Hasebe, K., Nishinari, K., Sugiyama, Y., Tadaki, S.-i., Yukawa, S., 2009. Metastability in the formation of an experimental traffic jam. *New J. Phys.* 11 (8), 083025.
- Nakhmani, A., Tannenbaum, A., 2013. A new distance measure based on generalized image normalized cross-correlation for robust video tracking and image recognition. *Pattern Recogn. Lett.* 34 (3), 315–321.
- Nam, H., Han, B., 2016. Learning multi-domain convolutional neural networks for visual tracking. In: Proceedings of the IEEE Conference on Computer Vision and Pattern Recognition (CVPR).
- Observatory, 2017. Minnesota traffic observatory: data acquisition and sensing. < <http://www.its.umn.edu/ProgramsLabs/MNTrafficObservatory/> > .
- OpenCV.org, 2016. Open source computer vision library. < <http://opencv.org/> > .
- Orosz, G., Wilson, E., Szalai, R., Stépán, G., 2009. Exciting traffic jams: nonlinear phenomena behind traffic jam formation on highways. *Phys. Rev. E* 80 (4), 046205.
- PEMS, 2018. Performance measurement system database. < <http://pems.dot.ca.gov/> > .
- Pena-Gonzalez, R.H., Nuno-Maganda, M.A., 2014. Computer vision based real-time vehicle tracking and classification system. In: Proceedings of the 57th IEEE International Midwest Symposium on Circuits and Systems (MWSCAS).
- Piccoli, B., Han, K., Friesz, T.L., Yao, T., Tang, J., 2015. Second-order models and traffic data from mobile sensors. *Transport. Res. Part C: Emerg. Technol.* 52, 32–56.
- Ponsa, D., Lpez, A., 2007. Cascade of classifiers for vehicle detection. In: Lecture Notes in Computer Science (Including Subseries Lecture Notes in Artificial Intelligence and Lecture Notes in Bioinformatics), 4678 LNCS, pp. 980–989. cited By 11.
- Punzo, V., Borzacchiello, M.T., Ciuffo, B., 2011. On the assessment of vehicle trajectory data accuracy and application to the next generation simulation (NGSIM) program data. *Transport. Res. Part C: Emerg. Technol.* 19 (6), 1243–1262.
- Punzo, V., Formisano, D., Torrieri, V., 2005. Part 1: Traffic flow theory and car following: nonstationary kalman filter for estimation of accurate and consistent car-following data. *Transport. Res. Rec.: J. Transport. Res. Board* 1934, 1–12.
- Rajamani, R., Choi, S.B., Law, B.K., Hedrick, J.K., Prohaska, R., Kretz, P., 1998. Design and experimental implementation of control for a platoon of automated vehicles. *AMSE J. Dyn. Syst. Meas. Control* 122 (3), 470–476.
- Ranjitkar, P., Nakatsuji, T., Kawamura, A., 2005. Experimental analysis of car-following dynamics and traffic stability. *Transport. Res. Rec.: J. Transport. Res. Board* (1934), 22–32.
- Redmon, J., Divvala, S., Girshick, R., Farhadi, A., 2016. You only look once: Unified, real-time object detection. In: Proceedings of the IEEE Conference on Computer Vision and Pattern Recognition, pp. 779–788.
- Rothery, R., Silver, R., Herman, R., Turner, C., 1964. Analysis of experiments on single-lane bus flow. *Oper. Res.* 12 (6), 913–933.
- Rothery, R.W., 2001. Car following models. *Rev. Traffic Flow Theory Monograph*.
- Russell, B.C., Torralba, A., Murphy, K.P., Freeman, W.T., 2007. Labelme: a database and web-based tool for image annotation. *Int. J. Comput. Vis.* 77 (1–3), 157–173.
- Schreuder, M., Hoogendoorn, S.P., Van Zuylen, H.J., Gorte, B., Vosselman, G., 2003. Traffic data collection from aerial imagery. In: Proceedings of the Conference on Intelligent Transportation Systems, 2003, vol. 1. IEEE, pp. 779–784.
- Schumaker, L.L., Dierckx, P., 1994. Curve and surface fitting with splines. *Math. Comput.* 63 (207), 427.
- Serra, J.P., 1982. Image Analysis and Mathematical Morphology. Academic Press.
- Shamoto, D., Tomoeda, A., Nishi, R., Nishinari, K., 2011. Car-following model with relative-velocity effect and its experimental verification. *Phys. Rev. E* 83 (4), 046105.
- Shladover, S.E., 1995. Review of the state of development of advanced vehicle control systems (avcs). *Veh. Syst. Dyn.* 24 (6–7), 551–595.
- Shruthi, S., 2011. Vehicle tracking using convolutional neural network. In: Proceedings of the World Congress on Engineering, vol. 2.
- Smith, S.A., 1985. Freeway data collection for studying vehicle interactions-technical report. Final report. Technical report, JHK & Associates.
- Stern, R.E., Chen, Y., Churchill, M., Wu, F., Delle Monache, M.L., Piccoli, B., Seibold, B., Sprinkle, J., Work, D.B., 2018. Quantifying air quality benefits resulting from few autonomous vehicles stabilizing traffic. *Transport. Res. Part D: Transport Environ.* 67 (2019), 351–365.
- Stern, R.E., Cui, S., Monache, M.L.D., Bhadani, R., Bunting, M., Churchill, M., Hamilton, N., Haulcy, R., Pohlmann, H., Wu, F., Piccoli, B., Seibold, B., Sprinkle, J., Work, D.B., 2018b. Dissipation of stop-and-go waves via control of autonomous vehicles: field experiments. *Transport. Res. Part C: Emerg. Technol.* 89, 205–221.
- Sugiyama, Y., Fukui, M., Kikuchi, M., Hasebe, K., Nakayama, A., Nishinari, K., Tadaki, S.I., Yukawa, S., 2008. Traffic jams without bottlenecks-experimental evidence for the physical mechanism of the formation of a jam. *New J. Phys.* 10 (3), 033001.
- Swaroop, D., Hedrick, J.K., 1996. String stability of interconnected systems. *IEEE Trans. Autom. Control* 41 (3), 349–357.
- Tadaki, S.-I., Kikuchi, M., Fukui, M., Nakayama, A., Nishinari, K., Shibata, A., Sugiyama, Y., Yosida, T., Yukawa, S., 2013. Phase transition in traffic jam experiment on a circuit. *New J. Phys.* 15 (10), 103034.
- Talebpour, A., Mahmassani, H.S., 2016. Influence of connected and autonomous vehicles on traffic flow stability and throughput. *Transport. Res. Part C: Emerg. Technol.* 71, 143–163.
- Teo, K.T.K., Chin, R.K.Y., Rao, N.S.V.K., Wong, F., Khong, W.L., 2014. Vehicle tracking using particle filter for parking management system. Proceedings of the 4th International Conference on Artificial Intelligence with Applications in Engineering and Technology 193–198.
- Thiemann, C., Treiber, M., Kesting, A., 2008. Estimating acceleration and lane-changing dynamics from next generation simulation trajectory data. *Transport. Res. Rec.: J. Transport. Res. Board* 2088, 90–101.
- Tian, J., Li, G., Treiber, M., Jiang, R., Jia, N., Ma, S., 2016. Cellular automaton model simulating spatiotemporal patterns, phase transitions and concave growth pattern of oscillations in traffic flow. *Transport. Res. Part B: Methodol.* 93, 560–575.
- Tordeux, A., Seyfried, A., 2014. Collision-free nonuniform dynamics within continuous optimal velocity models. *Phys. Rev. E* 90 (4), 042812.
- Treiber, M., Kesting, A., Thiemann, C., 2008. How much does traffic congestion increase fuel consumption and emissions? Applying a fuel consumption model to the NGSIM trajectory data. In: Proceedings of the 87th Annual Meeting of the Transportation Research Board.
- Treiterer, J., 1975. Investigation of traffic dynamics by aerial photogrammetry techniques. Final report EES278. Transportation Research Center, Department of Civil Engineering, Ohio State University.
- UMTRI, 2018. University of Michigan Naturalistic Driving Data. < <http://www.umtri.umich.edu/our-focus/naturalistic-driving-data> > .
- Vasconcelos, L., Neto, L., Santos, S., Silva, A.B., Seco, Á., 2014. Calibration of the gipps car-following model using trajectory data. *Transport. Res. Proc.* 3, 952–961.
- VTU, 2018. Virginia Technical University Naturalistic Driving Study Data. < <http://www.vtti.vt.edu/facilities/data-center.html> > .
- Wang, M., Daamen, W., Hoogendoorn, S.P., van Arem, B., 2016. Cooperative car-following control: distributed algorithm and impact on moving jam features. *IEEE Trans. Intell. Transport. Syst.* 17 (5), 1459–1471.
- Wang, N., Yeung, D.-Y., 2013. Learning a deep compact image representation for visual tracking. In: Burges, C.J.C., Bottou, L., Welling, M., Ghahramani, Z.,

- Weinberger, K.Q. (Eds.), Advances in Neural Information Processing Systems, vol. 26. Curran Associates, Inc., pp. 809–817.
- Wu, F., 2017. Ring Road Experiment Data and Source Code. < <https://doi.org/10.15695/vudata.cee.2> > .
- Wu, F., Stern, R.E., Churchill, M., Delle Monache, M.L., Han, K., Piccoli, B., Work, D.B., 2017. Measuring trajectories and fuel consumption in oscillatory traffic: experimental results. In: Proceedings of the 96th Transportation Research Board Meeting Annual Meeting.
- Zeroual, A., Messai, N., Kechida, S., Hamdi, F., 2015. Calibration and validation of a switched linear macroscopic traffic model. In: Proceedings of the 3rd International Conference on Control, Engineering & Information Technology (CEIT). IEEE, pp. 1–5.
- Zhou, Y., Nejati, H., Do, T.-T., Cheung, N.-M., Cheah, L., 2016. Image-based vehicle analysis using deep neural network: a systematic study. In: Proceedings of the IEEE International Conference on Digital Signal Processing.